

## VIROLOGY

# Common and species-specific molecular signatures, networks, and regulators of influenza virus infection in mice, ferrets, and humans

Christian V. Forst<sup>1,2,3,4†</sup>, Laura Martin-Sancho<sup>5†</sup>, Shashank Tripathi<sup>6†</sup>, Guojun Wang<sup>7</sup>, Luiz Gustavo Dos Anjos Borges<sup>4</sup>, Minghui Wang<sup>1,2,3</sup>, Adam Geber<sup>8</sup>, Lauren Lashua<sup>8</sup>, Tao Ding<sup>8</sup>, Xianxiao Zhou<sup>1,2,3</sup>, Chalise E. Carter<sup>9</sup>, Giorgi Metreveli<sup>4</sup>, Ariel Rodriguez-Frandsen<sup>5</sup>, Matthew D. Urbanowski<sup>4</sup>, Kris M. White<sup>4,10</sup>, David A. Stein<sup>11</sup>, Hong Moulton<sup>11</sup>, Sumit K. Chanda<sup>5</sup>, Lars Pache<sup>5</sup>, Megan L. Shaw<sup>4‡</sup>, Ted M. Ross<sup>9</sup>, Elodie Ghedin<sup>8,12\*</sup>, Adolfo García-Sastre<sup>4,10,13,14,15\*</sup>, Bin Zhang<sup>1,2,3\*</sup>

Molecular responses to influenza A virus (IAV) infections vary between mammalian species. To identify conserved and species-specific molecular responses, we perform a comparative study of transcriptomic data derived from blood cells, primary epithelial cells, and lung tissues collected from IAV-infected humans, ferrets, and mice. The molecular responses in the human host have unique functions such as antigen processing that are not observed in mice or ferrets. Highly conserved gene coexpression modules across the three species are enriched for IAV infection-induced pathways including cell cycle and interferon (IFN) signaling. *TDRD7* is predicted as an IFN-inducible host factor that is up-regulated upon IAV infection in the three species. *TDRD7* is required for antiviral IFN response, potentially modulating IFN signaling via the JAK/STAT/IRF9 pathway. Identification of the common and species-specific molecular signatures, networks, and regulators of IAV infection provides insights into host-defense mechanisms and will facilitate the development of novel therapeutic interventions against IAV infection.

## INTRODUCTION

Influenza A virus (IAV), a member of the *Orthomyxoviridae* family, is the causative agent of acute respiratory tract infections that affect 5 to 20% of the human population and cause 250,000 to 500,000 deaths per year worldwide (1). In pandemic years, IAV infection can lead to higher mortality rates; the 1918 Spanish influenza pandemic

was the most severe pandemic recorded to date (2). Although waterfowl are the natural hosts of IAV, the virus is capable of infecting a wide range of mammals, including humans and swine, in which several strains are well adapted. The common symptoms of influenza—the so-called “flu-like symptoms”—are likely mediated at least in part by the interferon (IFN) response triggered by the innate immune system’s detection of viral RNA (3). IAV RNA is sensed by the ubiquitous cytosolic DExD/H box RNA helicase RIG-I (or *DDX58*). This innate sensor recognizes the 5-triphosphate moiety at the end of double-stranded RNA, characteristic of the viral genome in many RNA viruses, including IAV (4, 5). Stimulation of RIG-I (retinoic acid-inducible gene I) results in its conformational change and binding to the signaling adaptor MAVS (mitochondrial antiviral-signaling protein), which leads to the activation of nuclear factor  $\kappa$ B (NF- $\kappa$ B) and IFN regulatory factor 3 (IRF3) transcription factors and transcriptional induction of type I and type III IFN. Both types of IFN stimulate the Janus kinase/signal transducer and activator of transcription (JAK/STAT) pathway that ultimately results in the expression of IFN-stimulated genes (ISGs), many of which have antiviral activities (6, 7). To counteract these activities, viruses encode multiple IFN antagonists that shortcut the sensing and IFN-induced pathways at multiple levels. Specifically, IAV proteins NS1, PA-x, PB1-F2, and PB2, among others, have been shown to down-regulate IFN responses in infected cells.

Physiological and genetic differences between species contribute to different host responses to pathogen infection (8, 9). For example, species variations in the innate immune responses to ligands can be nicely highlighted by three diverse innate immune receptors: Toll-like receptor 4 (TLR4), the NLRC4:NAIP (NLR family CARD domain-containing protein 4:NLR family of apoptosis inhibitory proteins) inflammasome, and nucleotide-binding oligomerization domain-containing protein 1 (NOD1). In the case of TLR4, which,

<sup>1</sup>Department of Genetics and Genomic Sciences, Icahn School of Medicine at Mount Sinai, One Gustave L. Levy Place, New York, NY 10029, USA. <sup>2</sup>Mount Sinai Center for Transformative Disease Modeling, Icahn School of Medicine at Mount Sinai, One Gustave L. Levy Place, New York, NY 10029, USA. <sup>3</sup>Icahn Institute for Data Science and Genomic Technology, Icahn School of Medicine at Mount Sinai, One Gustave L. Levy Place, New York, NY 10029, USA. <sup>4</sup>Department of Microbiology, Icahn School of Medicine at Mount Sinai, 1468 Madison Avenue, New York, NY 10029, USA. <sup>5</sup>Infectious and Inflammatory Disease Center, Sanford Burnham Prebys Medical Discovery Institute, 10901 North Torrey Pines Road, La Jolla, CA 92037, USA. <sup>6</sup>Centre for Infectious Disease Research, Department of Microbiology and Cell Biology, Indian Institute of Science, Bengaluru 560012, India. <sup>7</sup>The State Key Laboratory of Reproductive Regulation and Breeding of Grassland Livestock, College of Life Sciences, Inner Mongolia University, Hohhot, People’s Republic of China. <sup>8</sup>Center for Genomics and Systems Biology, Department of Biology, New York University, 12 Waverly Place, New York, NY 10003, USA. <sup>9</sup>Department of Infectious Diseases, Center for Vaccines and Immunology, University of Georgia, Athens, GA 30602, USA. <sup>10</sup>Global Health and Emerging Pathogens Institute, Icahn School of Medicine at Mount Sinai, 1468 Madison Avenue, New York, NY 10029, USA. <sup>11</sup>Department of Biomedical Sciences, College of Veterinary Medicine, Oregon State University, Corvallis, OR 97331, USA. <sup>12</sup>Systems Genomics Section, Laboratory of Parasitic Diseases, NIAID, NIH, Bethesda, MD 20892, USA. <sup>13</sup>Department of Medicine, Division of Infectious Diseases, Icahn School of Medicine at Mount Sinai, 1468 Madison Avenue, New York, NY 10029, USA. <sup>14</sup>The Tisch Cancer Center, Icahn School of Medicine at Mount Sinai, 1468 Madison Avenue, New York, NY 10029, USA. <sup>15</sup>Department of Pathology, Molecular and Cell-Based Medicine, Icahn School of Medicine at Mount Sinai, 1468 Madison Avenue, New York, NY 10029, USA.

\*Corresponding author. Email: bin.zhang@mssm.edu (B.Z.); adolfo.garcia-sastre@mssm.edu (A.G.-S.); elodie.ghedin@nih.gov (E.G.)

†These authors contributed equally to this work.

‡Present address: Department of Medical Biosciences, University of the Western Cape, Robert Sobukwe Road, Bellville 7535, South Africa.

in conjunction with myeloid differentiation factor 2 (MD-2), responds to lipopolysaccharide (LPS), fascinating observations have been made regarding the different agonistic and antagonistic behaviors of ligands when recognized by the human, mouse, and horse orthologs of the receptor. LPS from *Rhodobacter sphaeroides* is an agonist in horses and an antagonist in humans and mice. Similarly, LPS from *Escherichia coli* functions as an agonist in horses and mice, but as an antagonist to human TLR4:MD-2 activation (10). Another example is the poor correlation between human and murine inflammatory transcriptomic responses (11), or the species specificity of many viral IFN antagonistic mechanisms (12). However, the cornerstone of modern biomedical research still relies on the use of animal models to explore basic pathophysiological mechanisms, evaluate new therapeutic approaches, and make go or no-go decisions to carry new drug candidates forward into clinical trials. A better understanding of IAV-host responses in different mammalian species, including multiple animal models widely used in influenza research, would provide insights into the commonalities and differences of the host immune responses to IAV infection, as well as the common and specific host factors that contribute to enhanced disease severity or resilience.

Here, we carry out a comprehensive comparative study of RNA sequencing (RNA-seq) data derived from blood, primary epithelial cells, and lung tissues collected from IAV-infected humans, ferrets, and mice to identify conserved and species-specific molecular responses to IAV infection. Deciphering species-specific host factors, pathways, and host defense processes triggered by different viral strains are critical for understanding the pathophysiology of IAV infection. The key host-defense processes and the host factors identified in this study pave the way to developing more effective therapeutic interventions. Furthermore, the information derived from this study can be leveraged to assess the relevance of animal models to humans in IAV infection.

## RESULTS

To identify key molecular processes shared by and specific to humans, ferrets, or mice infected with IAV, we analyzed a large amount of

mRNA-seq data from human whole blood, human tracheobronchial epithelial (HTBE) cells, human monocyte-derived macrophages (MDMs), ferret blood, ferret lung, and mouse lung, infected with influenza A/California/07/2009(H1N1) virus. Time series data were collected over a period of 24 hours in the case of cell culture infection, 4 days for mice, and 14 days for ferrets (see Table 1). Figure 1 provides an overview of the analytical framework (see also fig. S1). The goals of this study were to identify conserved and species-specific molecular responses triggered by IAV and to further determine pan-tissue and tissue-specific responses to IAV infection across different hosts (for an overview of species, tissues, and systems, see table S1). We hypothesize that immune and host defense responses to IAV infection have both commonalities and differences between different species. IAV not only primarily infects the respiratory tissue but also induces a systemic response in the blood. IAV infection is likely to trigger similar pathways (induction of ISGs by secreted IFN) and distinct unique pathways (due to local responses) in both tissues.

### IFN-related signaling and host defense are commonly up-regulated processes by IAV across species

Given eight different systems as combinations of three tissues (including cell culture, blood, and lung tissue) and three species (Table 1), we performed comparative analyses at multiple levels (see Materials and Methods). In particular, we were interested in the temporal response of gene expression patterns. For this purpose, we used two measures, a generalized linear model across time series to identify differentially expressed genes (DEGs) across the time series termed significantly expressed response genes (SRGs) and Jonckheere trend analysis (JTA) to identify significantly up- or down-regulated genes [Jonckheere trend genes (JTGs)] across the early measured time points (see Materials and Methods for both). The numbers of SRGs and JTGs are shown in Table 2, and their intersections are shown in the Venn diagrams in figs. S2 and S3.

Up-regulated processes in the lung are predominantly responsible for IFN-related signaling and response to cytokines and host defense. Other up-regulated processes involve the cell cycle and cell division required for the viral life cycle. The lung shared 30 up-regulated

**Table 1. Description of datasets used in this study.**

Reference	Organism	Tissue	# Samples	Time points	Dim	Comments
gn40 GSE40012 subset	Human	Whole blood	75	1, 2, 3, 4, and 5	Days	Uninfected patients days 1 and 5
HTBE	Human	Tracheobronchial epithelial cells	10	3, 6, 12, 18, and 24	Hours	Mock infection data at every time point
MDM	Human	Monocyte-derived macrophages	8	3, 6, 12, and 18	Hours	Mock infection data at every time point
ferretBs	Ferrets	Blood, serial	24	3, 5, and 8	Days	Mock infection at day -2
ferretBl	Ferrets	Blood, longitudinal	24	1, 3, 5, 8, and 14	Days	Mock infection at days -2 and 8
ferretLB	Ferrets	Upper lung	24	1, 3, 5, 8, and 14	Days	Mock infection at days -2 and 8
ferretLE	Ferrets	Lower lung	24	1, 3, 5, 8, and 14	Days	Mock infection at days -2 and 8
Mouse	Mice	Lung	21	0.5, 1, 2, 3, and 4	Days	Mock infection at day 0

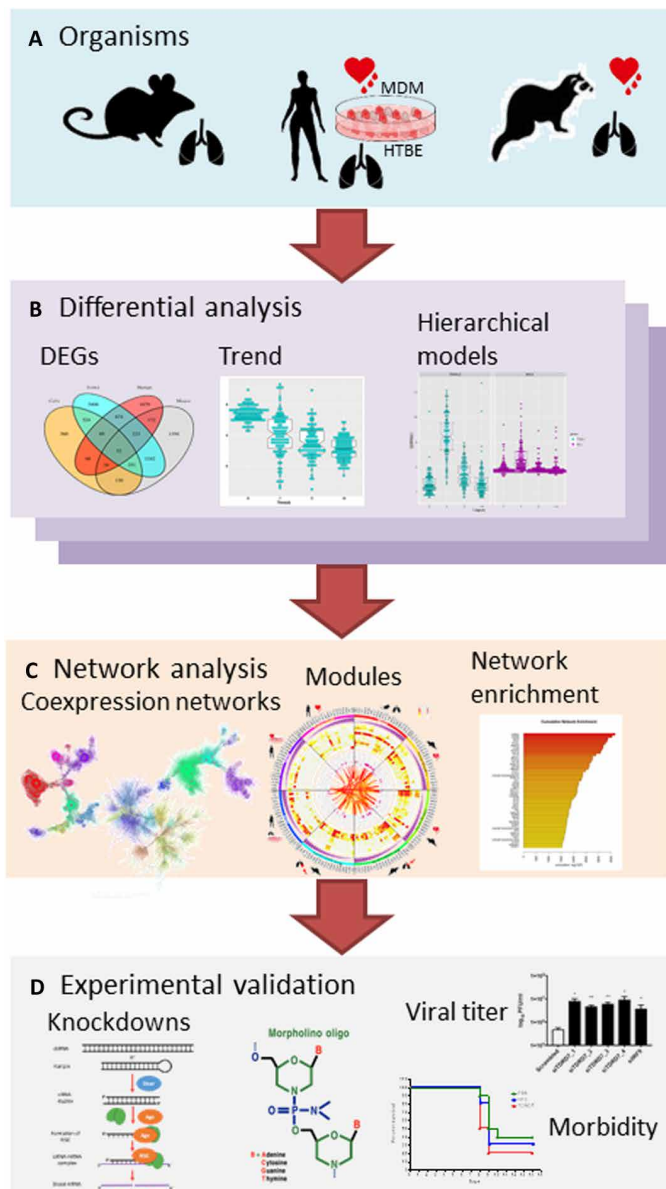


**Fig. 1. Flowchart of the cross-species analyses.** (A) Transcriptomic data from mouse lungs, human blood, MDM, and HTBE cells as well as ferret blood and lungs. (B) Differential expression analyses to identify differentially expressed genes (DEGs), significantly expressed response genes (SRGs), and Jonckheere trend genes (JTGs). (C) Network analysis to identify and prioritize network modules. (D) Predicted targets are validated by knockdown (KD) experiments and induced phenotypic response.

JTGs across all three species, including ISGs such as *ISG20*, *MX1*, and *OASL* (Fig. 2, A and B, and fig. S4). Up-regulated processes in the blood involve the immune system, particularly neutrophil activation, as well as intracellular, cytosolic vesicles (Fig. 3, A and B, and fig. S6) with 59 up-regulated JTGs common to all three species. While the down-regulated genes in the lung are involved in apoptosis and processes that might be inhibited by the virus to prevent interference with viral replication (Fig. 2, C and D, and fig. S5), the down-regulated genes in the blood were moderately enriched for

**Table 2. Differentially expressed genes [see also figs. S1 (A, C, and D) and S2 (A, C, and D)].**

Species/tissues	SRGs	JTGs up	JTGs down
Ferret	12,896	5177	6263
Human	6200	2904	3539
Mouse	3298	1533	3931
Common	957	200	244
Blood	13,831	5940	6911
Lung	8118	3457	6408
Common	5979	1551	1937
Total	15,970	7846	11,382

known pathways such as T cell receptor signaling and splicing and mRNA processing (Fig. 3, C and D, and fig. S7). Table S2 lists the commonly up- and down-regulated genes in the lung and the blood.

Cross-regulated genes, which are up-regulated in one species but down-regulated in another species, are complementary to commonly up- or down-regulated. With three species and two directions (up and down), there are 57 combinations of intersections; 12 combinations yielded meaningful sets, with nonempty intersections. An interesting cross-regulated process between mice and human is the antigen-dependent B cell activation/allograft rejection pathway, which was up-regulated in mice and down-regulated in humans. On the other hand, the complementary cross-regulated scenario identified respiratory chain and oxidoreductase activity, which was up-regulated in humans and down-regulated in mice (see fig. S8).

### The response in similar tissues across species is well preserved

We then carried out a side-by-side cross-species comparison analysis at the level of individual species (see Supplementary Text and figs. S9 to S11). Figure S12 shows the comparison of SRG signatures from eight model systems using the SuperExact Test (tables S3 and S4) (13). The lungs and blood in the ferret shared most SRGs [Fisher's exact test (FET)  $P < 1 \times 10^{-308}$  10.4 fold enrichment (FE)]. SRGs had stronger tissue specificity than species specificity. For example, although the most significant intersections between the mouse and ferret involved both ferret blood and lung SRGs, the overlap between the SRG signatures in mouse and ferret lungs was more significant than that between the mouse and ferret blood. Similarly, the SRG signature in the MDM cells overlapped that from ferret blood more significantly than the one from the HTBE cells, while the signature from the HTBE cells had a more significant overlap with those from the ferret and mouse lung than the one from the MDM cells. Such a trend was further supported by tissue-specific clustering analysis of the eight systems. Gene ontology (GO) analysis of individual signatures and their intersections revealed typical biological processes involved during IAV replication including type I IFN response/signaling, cell cycle, viral (transcription) process, intracellular location, and antigen processing/presentation. In summary, the analysis of common DEGs across all species shows a well-known picture of up-regulated IFN response and cell cycle control along with down-regulated apoptotic processes.





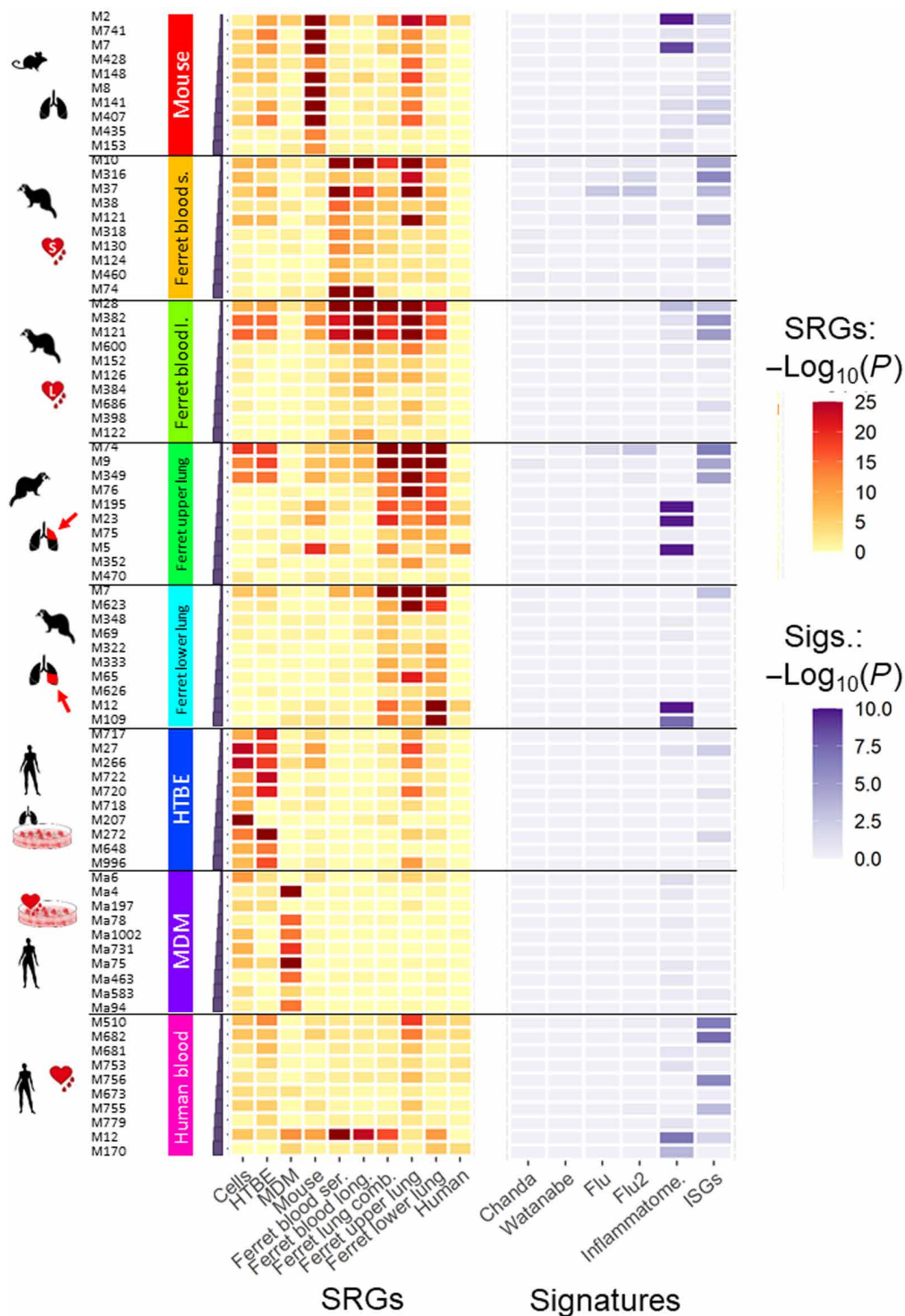


**Fig. 4. Enrichment of DEG signatures in the top 10 gene modules from each of the eight systems including mouse lung, ferret serial blood, ferret longitudinal blood, ferret lower lung, ferret upper lung, HTBE cells, human MDM, and human blood.** The leftmost labeled color bar refers to a particular system. The left heatmap shows significance levels of enrichment for the DEG signatures in HTBE and MDM cells combined, HTBE, MDM, mouse, ferret blood serial, ferret blood longitudinal, ferret lung combined, ferret upper lung, ferret lower lung, and human. The right heatmap shows the enrichment of several known influenza signatures [Chandra (59), Watanabe (58), the Flu and Flu2 signatures derived from Ward *et al.* (64), inflammatome, and ISGs; see table S23] in the top modules of the eight systems.

more genes (of 255 possible). As expected and consistent with the findings discussed above, cell cycle and IFN signaling were processes common to the top-ranked modules in the eight systems. Two examples of the modules enriched for commonly up-regulated genes are a mouse lung module M8 associated with IFN- $\alpha$  signaling (Fig. 2E) and a human blood module M12 involved in cytokine signaling/regulation of innate immunity (Fig. 3E). Examples of the modules enriched for commonly down-regulated genes include a mouse module M289 involved in the monocarboxylic acid catabolic process (Fig. 2F) and a human blood module M36 involved in graft

versus host response (Fig. 3F). Most of these modules were enriched for ISGs and inflammation signatures. As an example, Fig. 5 shows three lung (ferret, mouse, and HTBE) modules and one ferret blood-based module. All of these modules were highly ranked (fifth or higher), and they shared *DDX48* and Tudor Domain Containing 7 (*TDRD7*). *TDRD7* is an ISG that has recently been found to inhibit adenosine monophosphate-activated protein kinase (*AMPK*), required for herpes simplex virus replication (15), and, successively, autophagy, a process that is essential for paramyxovirus replication (16). The most conserved interactions in the lung networks include

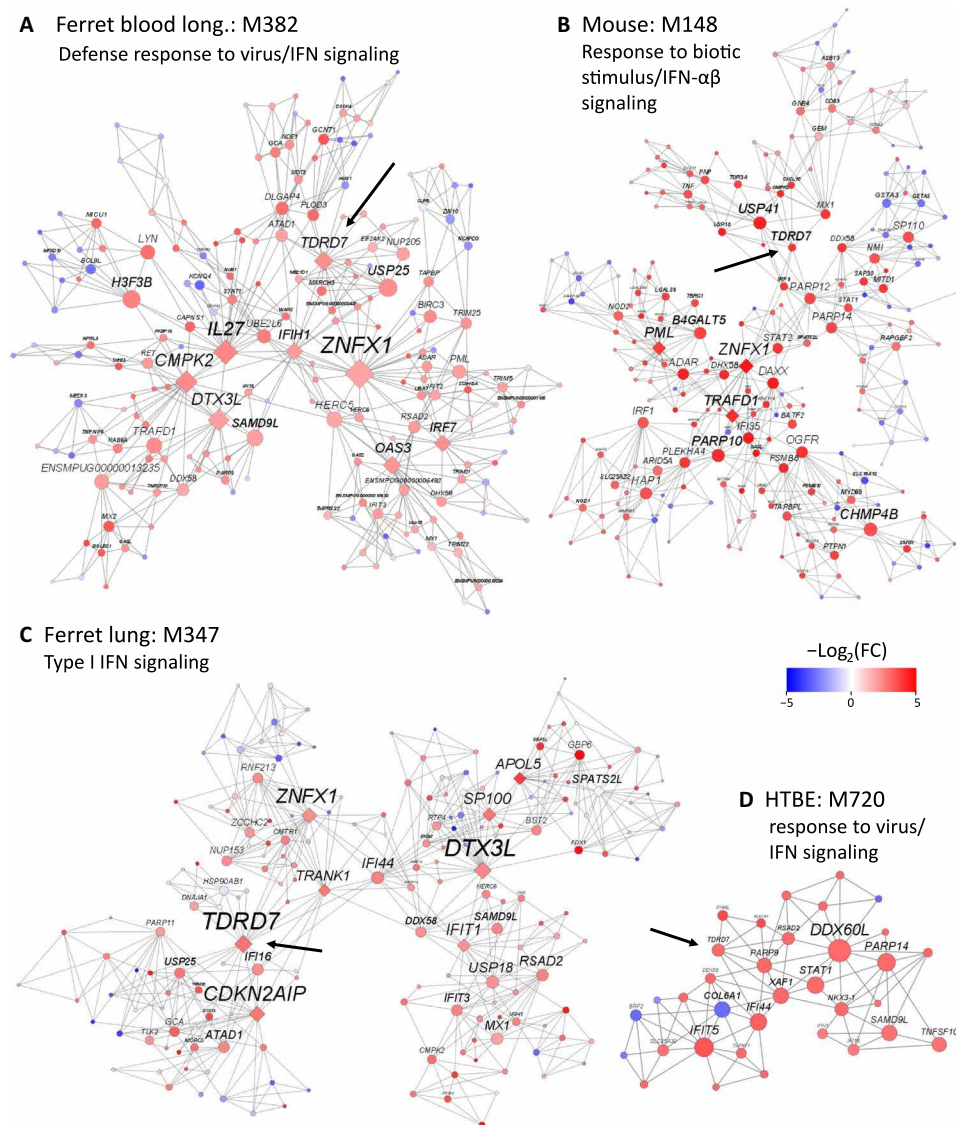


**Fig. 5. *TDRD7*-centered modules in three systems, ferret (blood and lung), mouse lung, and HTBE.** Modules with *TDRD7*-centered MEGENA networks are shown involving IFN signaling. Red nodes denote up-regulation, and blue nodes are down-regulated. Diamond-shaped nodes are key regulators. **(A)** The number two ranked ferret blood module M382, responsible for defense response to virus/IFN signaling, consists of 204 nodes and 595 edges. Prominently displayed are the key regulators *CMPK2*, *DTX3L*, *IFIH1*, *IL27*, *IRF7*, *OAS3*, *TDRD7*, and *ZNF1*. **(B)** Another example is the number five ranked mouse module M148 (response to biotic stimulus/IFN- $\alpha$  signaling), with 223 nodes and 644 edges. Key drivers are *PML*, *TRAFD1*, and *ZNF1*. **(C)** The number two ranked ferret lung module M347 (type I IFN signaling) with 193 nodes and 554 edges involve key regulators *APO5*, *CDKN2AIP*, *DTX3L*, *ENSMYPUG0000020197* (putative *IFIT1*), *SP100*, *SPATS2L*, *TDRD7*, *TRANK1*, and *ZNF1*. Overall, common nodes between modules (A to C) are *ATP10A*, *BST2*, *CMPK2*, *DDX58*, *EIF2AK2*, *ISG15*, *MX1*, *OASL*, *PARP12*, *STAT2*, *TDRD7*, and *ZNF1*. **(D)** The smaller, number five ranked HTBE module with 34 nodes and 95 edges is responsible for response to virus/IFN signaling. Key regulators in this module are *COL6A1* and *DDX60L*. Common nodes among all four modules include *DDX58* and *TDRD7*.

ISGs such as *IFI16*, *ZNF1*, and *ATAD1*. *ATAD1* (AAA adenosine triphosphatase) is responsible for mitochondrial quality control by extraction of mislocalized proteins from the mitochondrial membrane and indirectly preventing autophagy (17).

To investigate the biological relevance of key regulatory elements, we used both local (i.e., key regulators) and global (network) approaches. As described above, we first identified module-based key regulators (e.g., key genes and their corresponding proteins) from the top-ranked MEGENA modules. Thirty-one key regulators that are common between the three species were identified (fig. S2B and table S8). However, the ranks of these common key regulators varied significantly between species. Only *CDK1*, *CHD3*, *CLSPN*, *CSF1R*, *FCGRT*, *GMPPB*, *IRF7*, *OAS3*, *PSAP*, *STAU1*, and *TGFBI* were key regulators in the modules with ranks between 1 and 21 for all three species. Both *IRF7* and *OAS3* are the only two genes that were key regulators in the top-ranked modules across all three species. Both genes were significantly up-regulated (and later returned to baseline) in all the species and tissues, except for the human blood (figs. S14 and S15). Intersections of the key regulators from different scenarios are shown in figs. S2B to S6B. We further used a global network enrichment analysis to identify key regulators, termed network-enriched (NWE) regulators, whose network neighborhoods were significantly enriched for SRGs and JTGs. For each system, the network neighborhood of a candidate regulator in the respective global MEGENA network was intersected with the corresponding system-specific SRGs and JTGs, and the significance level was assessed by FET. Table S9 lists the network enrichment information together with the module assignment for 30,490 genes or probes. On the basis of a strict FET *P* value cutoff of  $1 \times 10^{-100}$ , *TDRD7* and *SP100* are the only NWE regulators across all the systems, while *TDRD7* is the top-ranked NWE regulator according to the cumulative score [ $\Sigma -\log_{10}(P) = 3663.1$ ; table S10 and fig. S16]. Both *TDRD7* and *SP100* were up-regulated in all the systems (figs. S17 and S18). Other top-ranked NWE regulators were antiviral genes including *DDX58*, *OAS3*, and *IFIH1* among other ISGs (table S11). All the NWE regulators except *DDX58* are also module-based key regulators in the respective MEGENA modules (see table S12).

We further analyzed the genes in the imminent network neighborhoods of *TDRD7* using the MEGENA networks from all eight systems. The intersections between *TDRD7*'s network neighborhoods in all the species were significant (table S13). Functional enrichment of the intersection indicates ISG-enriched IFN signaling, suggesting that the functional response of *TDRD7* upon influenza infection is triggered by IFN. An additional indication of the antiviral property of *TDRD7* and the processes potentially modulated by this factor were obtained from published protein-protein interactions based on experimental evidence (18). The *TDRD7* protein has been shown to function in a protein complex, together with *TACC1*, microtubule-associated chTOG (colonic and hepatic tumor over-expressed protein), Aurora A serine/threonine kinase, and the mRNA regulator *LSM7* (Like-Sm protein 7). Expressed RNAs of these proteins are colocalized in coexpression modules of all the three species studied. The *TDRD7*-*TACC1*-chTOG-Aurora A complex is instrumental in the regulation of microtubule dynamics, particularly with respect to mitotic spindle organization and cell division (19). *TDRD7* inhibits autophagy as an antiviral response (16). Another potential antiviral process regulated by *TDRD7* may originate from its association with mRNA regulatory LSMs (19). *TDRD7* interacts with *LSM7* in a complex with other LSMs. Both LSMs (20) and *TDRD7* (21) are

known to be members of RNA degrading cytosolic foci (such as RNA granules), particularly processing bodies (PBs) (22) that are responsible for the decay of unwanted mRNAs as an antiviral response. In conclusion, *TDRD7* is an up-regulated host factor across different species and tissues upon IAV challenge, potentially through IFN signaling and a putative key regulator of antiviral processes.

### Species-specific processes are diverse and could explain unique responses during viral infections

Different species have different genetic and regulatory repertoires and, thus, may respond differently to a biological threat, such as a viral infection. Specific pathways in one species may contribute to its resilience and provide insight to develop novel therapeutic strategies for human. To identify species-specific processes in host-viral interactions at the gene, module, and pathway levels, we performed a multiscale comparative analysis between the different systems.

At the gene level, we considered two different scenarios: sequence-based unique genes (SUGs) and function-based unique genes (FUGs). For a given species *x*, SUGs are the genes in *x* that have no ortholog in any other species investigated in this study, while FUGs are those that have orthologs in other species but are functionally specific to *x* regarding responses to IAV infections. Function refers to differential expression and a prominent role in gene subnetworks associated with physiology and phenotypes induced by IAV infections. Orthologs have been assessed using the National Center for Biotechnology Information (NCBI) ortholog information.

The majority (97) of sequence-specific SRGs in human samples were found in the human blood data and predominantly up-regulated (Fig. 5). These genes, involved in the regulation of apoptosis and leukocyte activation, include *ArfGAP* and other ankyrin repeat genes (*ANKRD36* and *ANKRD36B*), *CARD16* and *CARD17*, golgins (*GOLGA8CP* and *GOLGA8EP*), *HLA-DRB3*, *HLA-DRB4*, *HLA-DRB6*, *hnRNPA1L2*, *hnRNPA1P10*, heat shock proteins, long intergenic nonprotein coding RNA (LINC), and ribosomal protein and other pseudogenes. Sequence-specific SRGs in MDM include antiviral apolipoprotein B mRNA-editing enzymes (*APOBEC: 3C*, *3D*, and *3F*), leukocyte immunoglobulin receptors (*LILR: A3*, *B1*, *B2*, and *P2*), *LINC*s, neutrophil cytosolic factors (*NCF1B*, *NCF1C*), ribosomal protein pseudogenes, small nucleolar RNA host genes (*SNHG: 10*, *12*, *15*, and *16*), and zinc finger proteins (ZNF). *LILR*s have no homologs in mice. Another human SUG is *IL37*, which was exclusively up-regulated in HTBE cells. Its expression increased by 38.7-fold at 6 hours ( $P = 0.028$ ) and then dropped to the baseline level at 12 hours. The SRG signature in MDM is associated with the regulation of transcription and gene expression. The SRGs in HTBE have 12 SUGs including up-regulated *APOBEC3F*, *DDX60L*, *HCG4*, *HCP5*, *LINC00324*, *RARRES3*, and *SAMD9* and down-regulated *DANCR* and *DNM1P46*, as well as *RPSAP52*, *SLC35E2*, and *ZSCAN12P1* with a variable expression (i.e., mixture of up- and down-regulations during temporal response). The SRGs in the ferret data have no functional annotation, and they include about 350 SUGs in the ferret blood. Similarly, the SUGs in the mouse were also largely poorly annotated but included well-known mouse genes (*Ifi2712a*, *Ifi47*, *Ifitm6*, *Ly6a/i*, *Trem3*, *Tlr11*, and *Tlr13*) and SRGs. However, the specific TLRs (*Tlr11* and *Tlr13*) are not the primary receptors to recognize the influenza virus.

Species-specific responses complement the conserved responses against influenza (fig. S19B). Notably, human-specific SRGs in the blood are prominently enriched for olfactory reception stimulus and signaling pathways, human leukocyte alleles (*HLA-DM* and *HLA-DR*),

and killer cell immunoglobulin-like receptors (*KIR2DL1/3*). The ferret FUGs in the ferret SRGs are enriched for cell adhesion molecules (*LICAMs*) involved in signal transduction by L1. The mouse FUGs in the mouse SRGs are associated with drug/xenobiotic metabolism by cytochrome P450 and glutathione metabolism (table S14).

Note that this study does not include RNA-seq data from the mouse blood. The FUGs of the up-regulated JTGs in the ferret blood were associated with vesicle transport, while those in human blood were enriched for structural constituents of ribosomal genes (table S15). The up-regulated JTGs in the blood shared by the human and ferrets are listed in table S16). The down-regulated JTGs in blood common to ferret and human were involved in the regulation of ribosomal RNA processing and T cell activation (fig. S7 and table S17). The ferret FUGs of the down-regulated JTGs in the ferret blood were involved in noncoding RNA metabolic processes, while the human FUGs of the down-regulated JTGs in the human blood were related to the positive regulation of response to stimulus (table S18). The up-regulated JTGs in both the ferret and the mouse lung were involved in the immune response, particularly IFN signaling, *CCR1/4* chemokine receptor binding, and cell cycle processes (fig. S4). The up-regulated JTGs at early time points during IAV infection observed in the human and mouse lung tissues were specifically involved in the innate immune response [TLR and IFN signaling and natural killer (NK) cell activation], consistent with the expected host responses during infection (table S19). The FUGs in the up-regulated JTGs in the mouse lung were involved in the defense response (table S20). Molecular processes involved in the down-regulated JTGs include apoptotic signaling (i.e., regulation of programmed cell death; fig. S4 and table S21). The FUGs of the down-regulated JTGs in the mouse lung were involved in sensory perception of smell, while those in the ferret lung were related to T cell activation (table S22).

In addition to the different genetic repertoire between the species (i.e., SUGs), functionally unique SRGs (i.e., FUGs) shape the species-specific response against IAV infection. However, the common molecular responses, e.g., orchestrated by the innate and adaptive immune system, still dominate the biological processes in response to IAV infection in the different hosts.

### Species-specific coexpression networks are involved in host defense and the viral life cycle

We then performed module conservation analysis to identify modules specific to each system and network enrichment analysis to identify common and species-specific network regulators (for details, see Methods and Materials). A gene whose network neighborhoods are significantly enriched for the respective DEGs or JTGs in one species but not in any other species is termed a uniquely network-enriched (UNWE) regulator. Compared to network modules common to all the systems, the modules specific to a system are smaller and less enriched for the respective DEG signatures and, thus, have lower ranks (table S24), indicating that the corresponding processes may be secondary to viral infection. Noteworthy is the human MDM-specific functional complex assembling the negative regulation of leukocyte activation and ESCRT I (endosomal sorting complex required for transport) complex/virus process regulation (Fig. 6A). Complement C3b/C4b receptor-like (*CRIL*), major histocompatibility complex (MHC) class I molecule *HLA-G*, RNA binding motif protein *RBM34*, and myeloid cell nuclear differentiation antigen (*MNDA*) are key regulators. All of these regulators and most of the genes in the module were up-regulated. Another module

unique to human lung cells (i.e., HTBE) is M103, the endocannabinoid signaling pathway (and the regulation thereof) with a nucleotidase activity function (Fig. 6B), and one particular member gene is 5'-nucleotidase, cytosolic II (*NT5C2*), which itself was up-regulated, but its network neighborhood was significantly enriched for the down-regulated genes in HTBE (FET  $P = 1.6 \times 10^{-31}$ , 13.9-fold). Figure S20C shows the network enrichment scores for *NT5C2* in the ferret, the human, and the mouse. *NT5C2* is a key regulator in this particular module and is the second-highest connected gene after up-regulated *ZCCHC8*, another human UNWE regulator (HTBE: FET  $P = 1.6 \times 10^{-48}$ , 17.4-fold; fig. S20D) and a member of the nuclear exosome targeting (NEXT) complex (23), and down-regulated human UNWE regulator *VAT1* (HTBE: FET  $P = 9.2 \times 10^{-42}$ , 9.5-fold). The NEXT-Exosome promotes viral ribogenesis and infectivity (24) and is required for the influenza virus life cycle (25).

Modules unique to the mouse are involved in cyanate metabolic processes, sphingolipid signaling pathways, and the positive regulation of T cell cytokine production (Fig. 6C). Key regulators in the module involved in the down-regulated cyanate metabolic process are the dicarbonyl and L-xylulose reductase (*Dcxr*), mercaptopyruvate sulfurtransferase (*Mpst*), and transmembrane protein *Tmem106c*. Down-regulation of the module would indicate the attenuation of such a putative antiviral response potentially orchestrated by the detoxification enzyme *Mpst* (26). A key regulator in the down-regulated sphingolipid signaling pathway module is annexin A11 (*Anxa11*), a member of calcium-dependent phospholipid-binding proteins. *Anxa11* is essential to the cell cycle, apoptosis, vesicle trafficking, and signal transduction (27).

A "unique" ferret lung module is significantly enriched for the cell cycle and cytokinesis function (Fig. 6D). Key regulators in this up-regulated module include predominantly mitochondrial maintenance complex members, such as *MCM4* and *MCM10*, cell cycle regulatory maternal embryonic leucine zipper kinase (Melk), RhoGEF (Rho GTPase guanine nucleotide exchange factor) epithelial cell transforming 2 factor (*ECT2*), and marker of proliferation (*MKI67*). In the case of the H5N1 influenza virus, it has been shown that *MCM3*, *MCM4*, *MCM5*, and *MCM6* have close interactions with the viral polymerase (PA) protein, indicating the conserved function of PA-MCM interactions in the process of virus infection and replication (28). Thus, this particular ferret lung module is relevant for the influenza virus life cycle.

Similar to the investigation of key network regulators affecting common processes, we were interested in system-specific regulators. For this purpose, we investigated regulators whose network neighborhood is uniquely enriched by DEGs (fig. S21). One prominent example is *SPARC* (osteonectin), cwcv- and kazal-like domains proteoglycan 2 (*SPOCK2*). Induced in HTBEs and mouse lungs as well as ferret and human blood, this particular gene is highly and exclusively enriched in the human blood network (FET  $P = 1.8 \times 10^{-267}$ ). As a member of the antigen receptor-mediated signaling pathway, *SPOCK2* is a key regulator in the human blood together with three other human blood key regulators butyrophilin-like 3 (*BTNL3*; FET  $P = 2.4 \times 10^{-298}$ ), interleukin-2 receptor subunit  $\beta$  (*IL2RB*; FET  $P = 6.9 \times 10^{-271}$ ), and megakaryocyte-associated tyrosine kinase (*MATK*; FET  $P = 1.5 \times 10^{-305}$ ). The latter two regulators are also NWE regulators in the ferret, while *BTNL3* is not present in the ferret and mouse datasets. *SPOCK2* seems to be a binding partner of *DDX58*. Knockdown (KD) of *SPOCK2* was shown to enhance viral HA expression, suggesting its antiviral role (29). *SPOCK2* was recently shown to protect lung epithelial cells against virus infections (30).

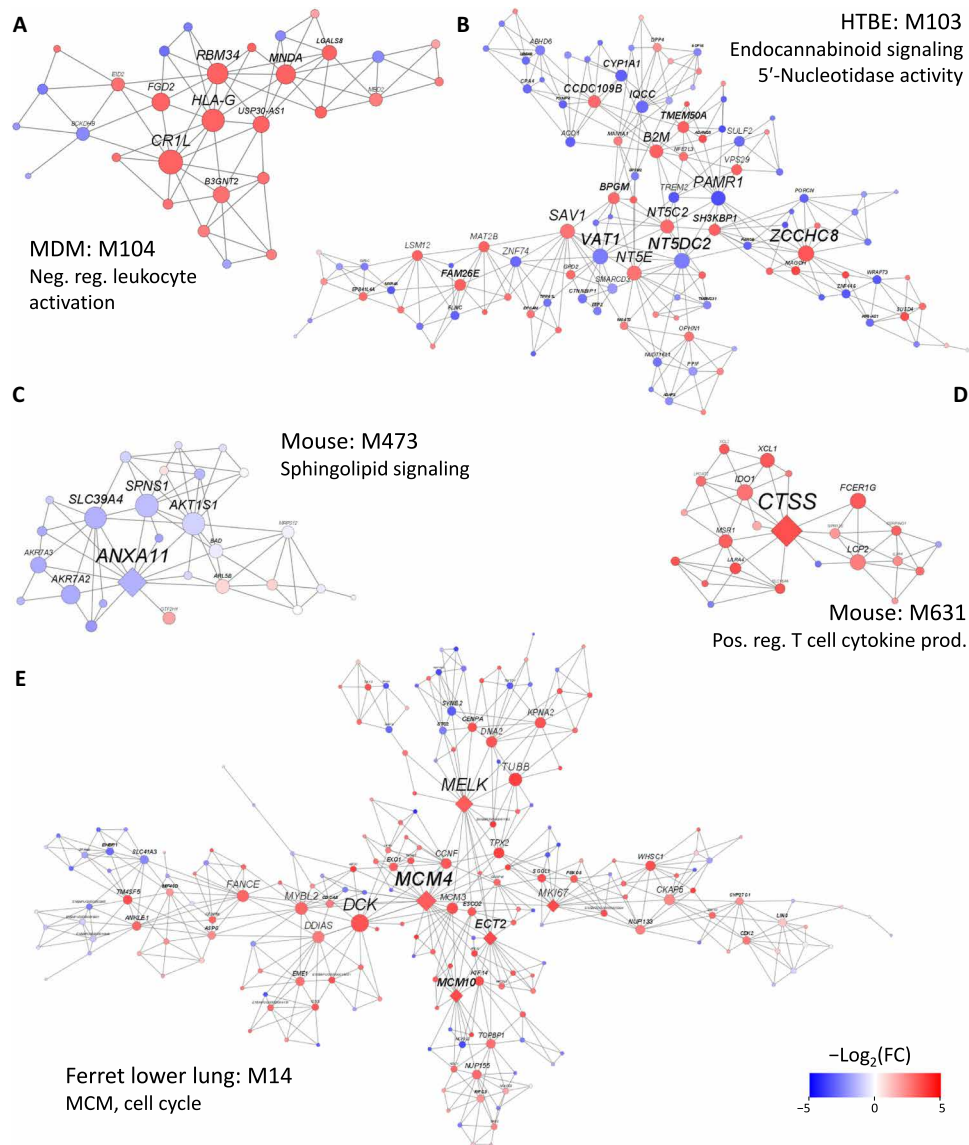


**Fig. 6. Species unique MEGENA modules.** Unique network modules in (A) human MDM cells, (B) HTBE cells, (C and D) mouse lung, and (E) ferret lower lung are shown. Red nodes denote up-regulation, and blue nodes denote down-regulation. Diamond-shaped nodes are key regulators. Species unique MEGENA modules were identified by enrichment for SRG (JTG) intersection signatures from all eight systems. Modules with significant enrichment in one species but not in any other were deemed unique. (A) The human (MDM) M104 unique module with 30 nodes and 78 edges is ranked number 75 and is responsible for the negative regulation of leukocyte activation. *CR1L*, *HLA-G*, *MNDA*, and *RBM34* are key regulators in this module. Most of the genes in this pathway are up-regulated. (B) The number 67 ranked regulation of endocannabinoid signaling/endosomal vacuolar pathway with 114 nodes, 326 edges, and key regulators *HDGFRP2*, *PDGFC*, *SMPDT*, *TIPARP*, *TJAP1*, and *U2AF2* is shown. (C) The number 136 ranked and predominantly down-regulated mouse module M473 relevant for sphingolipid signaling has 27 nodes and 67 edges. The sole key regulator is *ANXA11*. (D) M631 is a number 49 ranked and up-regulated mouse module responsible for positive regulation of T cell cytokine production with *CTSS* as a single key regulator. M631 has 23 nodes and 57 edges. (E) The number 170 ranked ferret lower lung module M14 with 202 nodes and 565 edges shows minichromosome maintenance (MCM) and cell cycle functionality. Key regulators are *ARHGAP21*, *ARPC1B*, *ATP6V0C*, *CD3D*, *CD3E*, *CD3G*, *CDC42BPG*, *CFL1*, *DPP3*, *ECT2*, *ENO1*, *ENSMPUG00000006004* (putative *MELK*), *ENSMPUG00000008504* (putative *TRBC2*), *IFT81*, *MCM10*, *MCM4*, *MKI67*, *TPPP3*, *TRAC*, *TRADD*, *UBE2V1*, and *UNC93B1*.

### TDRD7 KD increases IAV replication in vitro and in vivo

To confirm the role of *TDRD7* against IAV, we conducted a more comprehensive assessment of the effect of *TDRD7* during infection. After validating that efficient *TDRD7* KD (Fig. 7A) did not induce small interfering RNA (siRNA)-mediated toxicity in human cells (Fig. 7B), we tested the impact of *TDRD7* KD on influenza virus growth. Depletion of *TDRD7* increased the number of viral particles

released into the supernatant by 5- to 10-fold (Fig. 7C). Next, we assessed whether *TDRD7* is stimulated upon type I IFN treatment, as previously reported (16). *TDRD7* mRNA levels increased in a dose-dependent manner in a variety of human cell types, including HTBE cells (Fig. 7D). Last, we used peptide-conjugated phosphorodiamidate morpholino oligomers (PPMOs) to investigate the impact of *TDRD7* depletion in vivo. Treatment of mice with

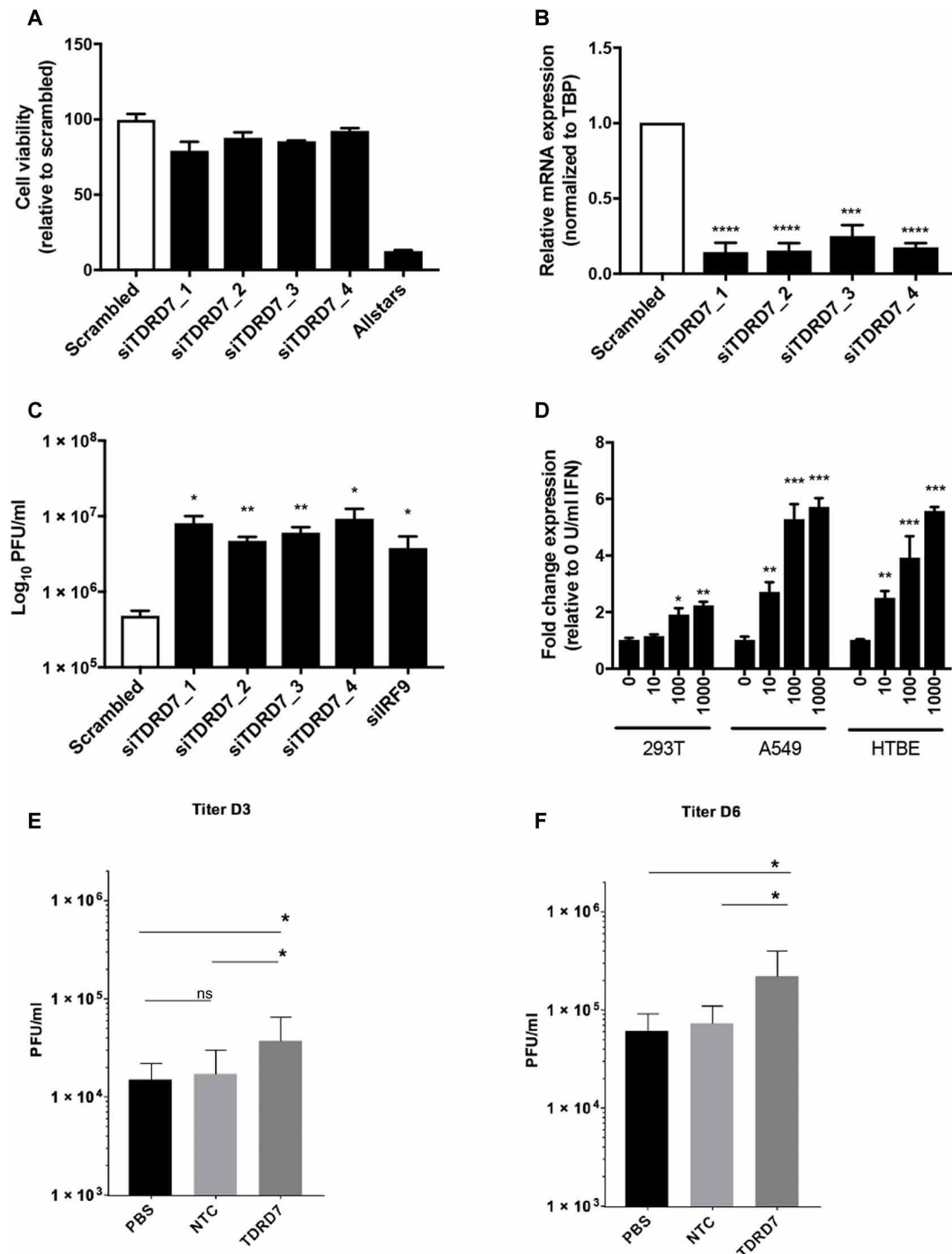


**Fig. 7. TDRD7 KD increases IAV replication in vitro and in vivo.** A549 cells were transfected with four individual siRNAs targeting TDRD7, the negative control scrambled or the cytotoxic siRNA Allstars. At 48 hours after transfection, (A) RNA was isolated and analyzed by quantitative reverse transcription polymerase chain reaction (qRT-PCR) using primers specific for TDRD7 and TBP. (B) Cell viability was assessed using CellTiter-Glow. (C) A549 cells were transfected with indicated siRNAs. At 48 hours after transfection, cells were infected with WSN virus at a multiplicity of infection of 0.01. Supernatants were collected at 48 hours postinfection (hpi) and analyzed by plaque assay using MDCK cells. (D) A549, 293T, and HTBE cells were seeded overnight and then treated with increasing doses of universal IFN- $\beta$  (0, 10, 100, and 1000 IU/ml) for 24 hours. RNA was then isolated and analyzed by qRT-PCR using primers specific for TDRD7 and TBP. (A to D) Data represent means  $\pm$  SD of at least two independent experiments run in triplicate. \* $P$  < 0.05, \*\* $P$  < 0.01, \*\*\* $P$  < 0.001, and \*\*\*\* $P$  < 0.0001 by one-way analysis of variance (ANOVA) with Dunnett's post hoc test. Five-week-old female BALB/c mice were administered phosphate-buffered saline (PBS), nontargeting control (NTC), or TDRD7 PPMOs (100  $\mu$ g in 40  $\mu$ l of PBS; the equivalent of approximately 5 mg/kg) intranasally for two consecutive days before infection. On day 0, mice were infected with A/Puerto Rico/8/34 [40 plaque-forming units (PFU)] intranasally. On days 3 and 6 after infection, five mice per condition were euthanized to harvest the lungs and determine virus titer. The graph shows the mean lung virus titer  $\pm$  SD on day 3 (E) and day 6 (F) after infection. Data shown are from two independent experiments with five mice per condition. ns, not significant.

TDRD7-specific PPMOs resulted in a modest increase in morbidity as compared with phosphate-buffered saline (PBS) or nontargeting PPMO controls (fig. S22A), with no change in body weight (fig. S22B). Viral load in lungs from TDRD7 PPMO-treated mice was significantly higher compared to control mice challenged with either PBS or nontargeting PPMO, both at day 3 and day 6 after infection (Fig. 7, E and F). Overall, these data show that TDRD7 is an IFN-inducible factor whose depletion results in increased influenza virus growth both in vitro and in vivo.

We have further investigated the gene-regulatory program that is modulated by *TDRD7*. For this purpose, we compared the transcriptional response between wild type (WT; scrambled) and siTDRD7 KD (*TDRD7*<sup>KD</sup>) HTBE cells under mock, 12 hours, and 24 hours post influenza infection (hpi) (see Materials and Methods). Overall, 333 genes significantly change their expression pattern between mock and 24 hpi when comparing WT and *TDRD7*<sup>KD</sup> cells (i.e., differential expression between 24 hpi<sub>KD</sub> versus Mock<sub>KD</sub> and 24 hpi<sub>WT</sub> versus Mock<sub>WT</sub>). Two hundred seventy-three genes show a larger (positive) expression change between infected and mock in *TDRD7*<sup>KD</sup> cells than WT cells (*TDRD7*-restricted or *T*<sup>-</sup> genes), whereas 60 genes display larger expression change between infected and mock in WT cells compared to *TDRD7*<sup>KD</sup> cells (*TDRD7*-enhanced or *T*<sup>+</sup> genes). The largest siTDRD7 effect was experienced by *T*<sup>-</sup> gene neurotensin [*NTS*; log<sub>2</sub> fold change (log<sub>2</sub>FC) = 15.6, false discovery rate (FDR) = 0.039; fig. S23A], aldehyde dehydrogenase *ALDH1A1* (log<sub>2</sub>FC = 14.0, FDR = 0.035; fig. S23B), and G protein-coupled receptor 4 (*GPR4*; log<sub>2</sub>FC = 4.1, FDR = 0.015; fig. S23C). On the other hand, most responsive *T*<sup>+</sup> genes include myosin heavy chains *MYH6* and *MYH7* (log<sub>2</sub>FC = -8.6 and -6.5, FDR = 0.017 and 0.027, respectively; fig. S23, D and E) and tumor protein *TP73* (log<sub>2</sub>FC = -3.0, FDR = 0.015; fig. S23F). No significant change in expression pattern was observed when comparing KD and WT expression between 12 days postinfection (dpi) and mock. *T*<sup>+</sup> genes are enriched for the epidermal growth factor receptor (EGFR1) pathway (fig. S24A), tumor necrosis factor- $\alpha$  (TNF- $\alpha$ ) signaling via NF- $\kappa$ B, and response to metal ions, whereas *T*<sup>-</sup> genes are enriched for IL signaling (IL-2 and IL-18), TNF- $\alpha$  effect on cytokine activity, cell motility, and apoptosis (fig. S24B).

We were further interested in the specific transcriptional program that is modulated by *TDRD7*. For this purpose, we investigated the MEGENA network neighborhood of *TDRD7* for enrichment with *T*<sup>+</sup> and *T*<sup>-</sup> genes. As the individual system neighborhood was poorly enriched for *T*<sup>+</sup>/*T*<sup>-</sup> genes, we used consensus networks across all systems, as well as combining blood and lung systems separately. Overall, we considered network neighborhood up to layer 4 from the origin "*TDRD7*." However, with high connectivity, outer layers tend to cover the complete network. Thus, we restrict ourselves to maximum layers of two only for all systems and two and three for consensus networks in blood and lung systems. The network neighborhoods are chosen to control the number of included genes (half of the total number of genes at maximum). The *TDRD7* network neighborhood is mainly enriched for (RIG-I-mediated induction of) IFN signaling. However, we have identified other immune response pathways, such as JAK/STAT3 signaling or IL-2/IL-6 signaling.

To identify processes that are potentially directly mediated by *TDRD7*, we investigated the intersection between *TDRD7* network neighborhoods and *T*<sup>+</sup>/*T*<sup>-</sup> genes. Figure 8A shows multiple intersections between network layer 2 and *T*<sup>+</sup>/*T*<sup>-</sup> genes after SuperExact Test. Overall, the functional assessment of the network intersections with

*T*<sup>+</sup> genes is somewhat elusive because of the small number of genes (13 in the combined and 38 in the blood and lung network intersections). However, nonsignificant gene set enrichment indicates IFN-induced signaling and EGFR1 pathway functions (Fig. 8B). Network overlap with *T*<sup>-</sup> genes show a larger overlap with 50 genes in the combined, 159 in blood, and 168 in lung intersection, involving TNF- $\alpha$  signaling via NF- $\kappa$ B, IL-2/STAT5 signaling, IL-5 regulation of apoptosis, IL-6/JAK/STAT3, and unfolded protein response (Fig. 8C).

Key targets, i.e., targets that are a member of the network and *T*<sup>+</sup>/*T*<sup>-</sup> gene intersection and that themselves have a network neighborhood for enriched DEGs (see Materials and Methods), are as follows. *TDRD7*-enhanced (*T*<sup>+</sup>) key targets involve arrestin domain containing 3 (*ARRDC3*), as well as guanylate binding protein family member 1 and 6 (*GBP1* and *GBP6*). *ARRDC3* regulates G protein-mediated signaling. *ARRDC3* is a novel ISG and is up-regulated during SARS-CoV-2 (severe acute respiratory syndrome coronavirus 2) infection (31). It is known to suppress breast and prostate carcinoma by negatively regulating integrin  $\beta$ 4 (32, 33). *ARRDC3* further mediates G protein-coupled receptor lysosomal sorting and apoptosis-linked gene 2-interacting protein X [*ALIX*; or programmed cell death 6 interacting protein (*PDCD6IP*)]. *ALIX* is a Lys<sup>63</sup>-specific polyubiquitin binding protein that functions in retrovirus budding and dengue virus propagation (34, 35). However, *ARRDC3*'s expression, although differently expressed in WT compared to *TDRD7*<sup>KD</sup> cells, is significantly up-regulated during infection in both cell genotypes (fig. S25A). Thus, the effect of *TDRD7* via *ARRDC3* on the viral life cycle may only be moderate.

Other key targets are *GBP1* (fig. S25B) and *GBP6* (Fig. 8D). Both belong to the gene family of IFN-inducible guanosine triphosphatases (GTPases), which are involved in host resistance to pathogens among other well-known members, such as *MX1* (fig. S25C) and *MX2* (36). As transcriptomic *GBP6* response against influenza infection is almost eliminated in *TDRD7*<sup>KD</sup> cells at 24 hpi (except for a weak up-regulation at 12 hpi), an independent response of *TDRD7* and *GBP6* induced by IFN is rather unlikely. Thus, we conclude that *TDRD7* causative controls *GBP6* transcription. This control may potentially originate via modulation of the mRNA stability of IRFs. Although not a key target, we have identified another potential candidate of a *T*<sup>+</sup> gene in the network neighborhood of *TDRD7*, decapping mRNA 2 (*DCP2*); *DCP2* is a member of the mRNA degradation pathway in P-bodies together with cellular 5'-3' exoribonuclease 1 (*XRN1*) (37).

*TDRD7* potentially controls IFN levels via the mRNA degradation pathway, particularly involving *DCP2* expression during influenza infection. *DCP2* modulates the mRNA stability of IRF7 to regulate type I IFN response in antiviral innate immunity. Reduced levels of *DCP2* result in greater stability of *IRF7* mRNA corresponding to higher levels of IRF7 protein (38). Under WT conditions, *DCP2* expression increases at 24 hpi from low expression levels at 0 and 12 hpi. However, in *TDRD7*<sup>KD</sup> cells, *DCP2* maintains a high expression level independent of the infection condition (fig. S25D). We do not see such an effect of *DCP2* on *IRF7* expression (Fig. S25E). In addition, the expression of type I IFN, such as *IFNB1*, is only moderately affected by *TDRD7* (fig. S25F). However, we see a decrease of *IRF9* in *TDRD7*<sup>KD</sup> cells compared to WT cells (fig. S25G). The effect of *TDRD7* on the IFN pathway via potential *DCP2* regulation and mRNA decay control may then function via the JAK/STAT/IRF9 pathway. This effect is most pronounced at 24 hpi. For example, ISGs, such as *GBP6* and *MX1*, show significant up-regulation at this time point in WT cells. Under *TDRD7*<sup>KD</sup> conditions, IFN response

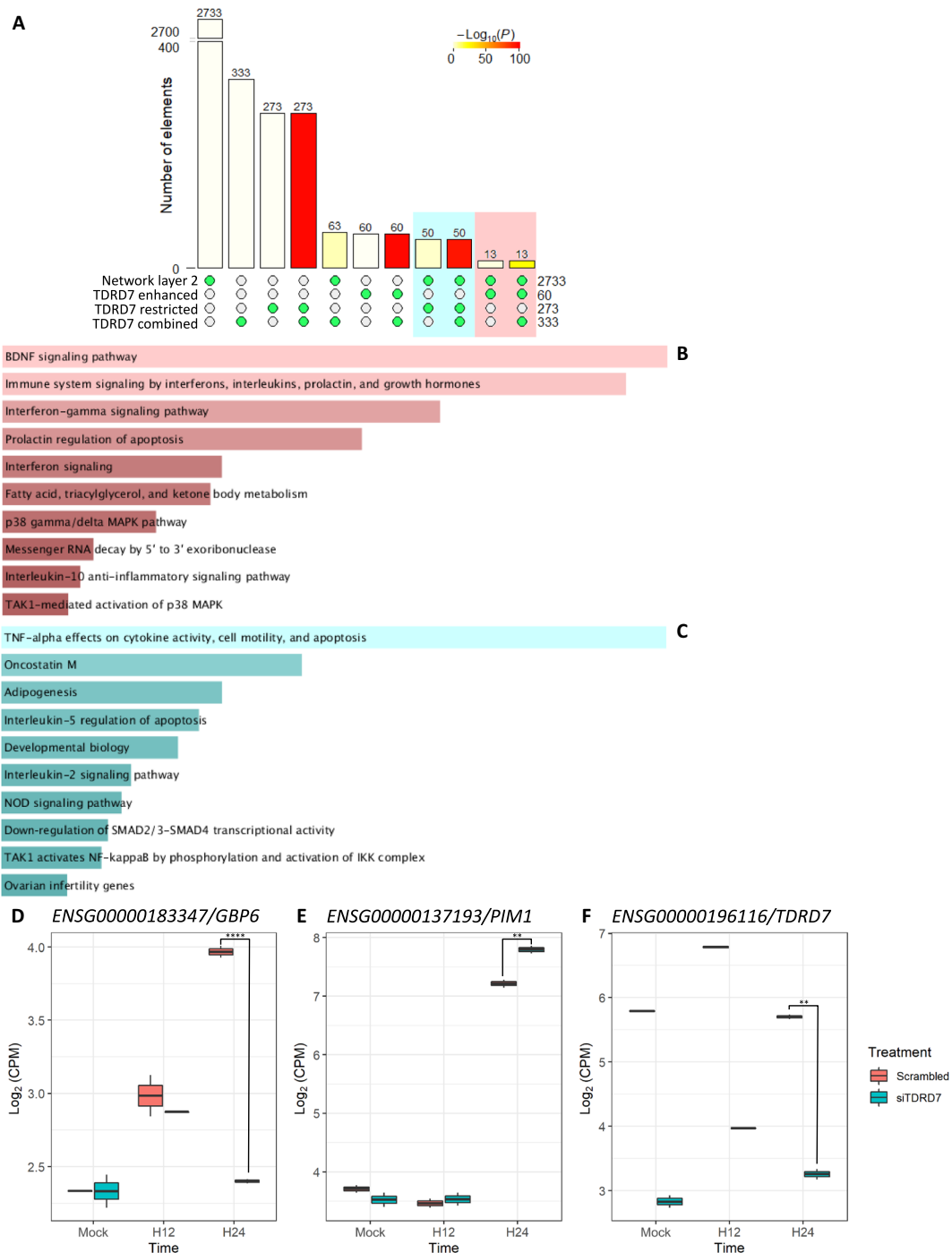


**Fig. 8. TDRD7 modulates IFN response.** The transcriptional response and induced biological processes during influenza infection in WT and TDRD7<sup>KD</sup> HTBE cells are shown. **(A)** The multisets intersections between the TDRD7 network neighborhood (up to layer 2) and significantly responding TDRD7 enhanced (T<sup>+</sup>) or restricted genes (T<sup>-</sup>) by SuperExact Test are depicted. The networks of all eight systems have been used to construct the consensus network. The layer 2 network neighborhood includes all next and second next neighboring genes of *TDRD7*. The heights of the bars indicate set size, and colors refer to FET *P* values (see scale). Green-filled circles below the bars denote corresponding intersected sets (left). The size of the network layer 2 ∩ T<sup>+</sup> intersection is 13 genes (red rectangle), whereas the network layer 2 ∩ T<sup>-</sup> intersection includes 50 members (blue rectangle). Both intersections are significant after FET (layer 2 ∩ T<sup>+</sup>: 2.28-fold enrichment (FE),  $P = 3.63 \times 10^{-3}$ ; layer 2 ∩ T<sup>-</sup>: 1.93-FE,  $P = 4.70 \times 10^{-6}$ ). The biological functions of the intersections have been assessed by functional enrichment for BioPlanet (2019) pathways. **(B)** The functional enrichment of *TDRD7*-enhanced genes in the network neighborhood (layer 2 ∩ T<sup>+</sup>) is shown involving IFN signaling. **(C)** The layer 2 ∩ T<sup>-</sup> intersection has TNF/NF-κB and IL signaling functionality. Two examples, one each of a T<sup>+</sup> and T<sup>-</sup> gene in the layer 2 neighborhood, are depicted. **(D)** Antiviral *GBP6* is an IFN-inducible guanosine triphosphatase (GTPase) that requires the IFN modulation by TDRD7 for significant up-regulation at 24 hpi. **(E)** *PIM1* is responsible for cell survival and may benefit the viral life cycle. **(F)** The expression of *TDRD7* in WT and TDRD7<sup>KD</sup> HTBE cells is shown. Significance between WT and TDRD7<sup>KD</sup> expression at 24 hpi is indicated as follows: \*\*\*\* $P < 0.001$  and \*\*\*\* $P < 0.0001$ , which was assessed using edgeR's generalized linear models together with a quasi-likelihood *F* test.

may be quenched by continuous depletion of IFN mRNA. We observed a change in expression between WT and TDRD7<sup>KD</sup> cells at 24 hpi of 2.99 FC (FDR =  $3.30 \times 10^{-5}$ ) for *GBP6* and of 1.57 FC (FDR =  $5.9 \times 10^{-4}$ ) for *MX1*. However, ISG expression may also be decreased via inhibition of JAK/STAT signaling. Although not significant, both *IRF9* and *STAT1* (fig. S25H) show reduced expression at 24 hpi in TDRD7<sup>KD</sup> cells compared to WT cells (IRF9: 1.46 FC, FDR = 0.16; STAT1: 1.37 FC, FDR = 0.010).

TDRD7-restricted key targets involve ADAM metallopeptidase domain 19 (*ADAM19*), B-cell lymphoma 2 (*BCL2*)-related protein A1 (*BCL2A1*), DLG (discs-large)-associated protein 4 (*DLGAP4*), EH domain containing 1 (*EHD1*), hexokinase 2 (*HK2*), and Pim-1 proto-oncogene (*PIM1*). *ADAM19* is a metallopeptidase that plays a role in cell-cell and cell-matrix interactions. *BCL2A1* has antiapoptotic activity and is directly controlled by NF- $\kappa$ B. *EHD1* regulates intracellular EGFR trafficking (39), a process hijacked by viruses for intracellular transport. *HK2* is another direct target of NF- $\kappa$ B. *PIM1* promotes cell survival by modulating the JAK/STAT and NF- $\kappa$ B activity [e.g., in primary mediastinal large B cell lymphoma PMBL cells (40)]. Down-regulated *PIM1* yields down-regulation of NF- $\kappa$ B- and STAT-dependent transcription of prosurvival factors, such as key target *BCL2A1* (40). Thus, we have identified a rather similar expression pattern of *BCL2A1* and *PIM1* in WT and TDRD7<sup>KD</sup> cells during influenza infection. Both *BCL2A1* (fig. S25I) and *PIM1* (Fig. 8E) show rather similar expression levels between WT and TDRD7<sup>KD</sup> cells, particularly at 12 hpi, with distinct higher expression under TDRD7<sup>KD</sup> conditions compared to WT at 24 hpi (*BCL2A1*: 3.0 FC, FDR = 0.040; *PIM1*: 1.69 FC, FDR = 0.29). Although we are restricted to transcriptomic response, of further interest with this respect is the indication of reduced virus production induced by inhibition of the *PIM1* kinase (41). This finding may indicate that *PIM1* abundance may support viral growth.

We have assessed the effect of TDRD7<sup>KD</sup> on *TDRD7* expression as a transcriptomic validation of our siRNA experiments. Figure 8F shows the temporal response in WT and TDRD7<sup>KD</sup> HTBE cells. Although *TDRD7* is expressed in TDRD7<sup>KD</sup> cells, we have observed a five- to eightfold change of *TDRD7* expression between WT and TDRD7<sup>KD</sup> cells (0 hpi: 7.8 FC, FDR = 0.019; 12 hpi: 7.0 FC, FDR = 0.0045; 24 hpi: 5.4 FC, FDR = 0.0088).

In conclusion, *TDRD7* co-modulates the IFN response, via either IRF mRNA control via *DPC2* or modulation of the JAK/STAT/IRF9 signaling pathway. This modulation is selective. It only affects IFN-inducible GTPases, such as *GBP1*, *GBP6*, *MX1*, or *MX2*. It also affects 2'-5'-oligoadenylate synthetases (OASs) or Viperin (*RSAD2*; fig. S25J). However, we have not observed a significant effect of *TDRD7* on other ISGs, such as IFIH1 (interferon induced with helicase C domain 1) (fig. S25K), IFI16 (fig. S25L), or the IFITMs. We have identified a second route for *TDRD7* as a novel antiviral factor. *TDRD7* may modulate cell survival factors, such as *PIM1* and *BCL2A1*, affecting the viral life cycle. This effect may be associated with the AMPK inhibition by *TDRD7*, identified by Subramanian *et al.* (15, 16). *PIM1* has been identified to block AMPK activation (42).

## DISCUSSION

In this study, we analyzed a large amount of transcriptomic data from influenza-infected humans, ferrets, and mice to profile their unique and conserved responses to IAV infection. We performed comparative analyses at multiple levels, ranging from differential expression,

multiscale gene coexpression networks, and key regulators. The most represented molecular response against IAV infection across all levels of complexity includes IFN signaling and the cell cycle. The cell cycle and its control by the virus are essential for viral replication. However, stimulation of the cell cycle may also be caused by the activation of the proliferation of immune cells. The IFN response and downstream signaling are the first lines of defense by the host against viral infections. ISGs and cell cycle genes are typically up-regulated in all the systems. Down-regulated genes and the corresponding processes involve apoptosis and adaptive immune response. Noticeable is the strong conservation of the DEGs and molecular processes in the same tissue across different species in contrast with the relatively weak conservation across different tissues within each species. For example, the overlap between the DEG signatures in human lung cells and ferret lung tissue is far more significant than the overlap between the DEG signatures from the different tissues in ferrets. A potential reason for the similarity observed between ferret blood and lung tissue is the sampling technique. At the time of the sacrifice of ferrets, blood was collected from the vein near the lungs. One exception is with human blood and MDM cells. The DEGs from the human blood highly significantly overlap those from ferret blood and lung SRGs (FET  $P < 1 \times 10^{-308}$ , 9.9-fold) as well as the human blood-based primary cells MDM (FET  $P = 4.6 \times 10^{-306}$ , 47.6-fold). Tissue-biased "preferences" were also observed in the case of key targets. The top-ranked NWE regulators, such as ISG *SP100* and the antiviral factor *TDRD7*, were expressed in all the systems. We validated the antiviral effect of *TDRD7* on influenza replication both in vivo and in vitro. siRNA-mediated KD of *TDRD7* in human lung A549 cells showed significantly increased release of IAV particles. These are robust results based on the commonly accepted criteria such as *P* value and effect size thresholds (see Materials and Methods) for all the datasets analyzed in this study.

Similarly, *TDRD7* KD in mice resulted in increased viral load in mouse lungs and increased morbidity. *TDRD7* is prominently placed in modules with IFN signaling functions together with other antiviral ISGs (Fig. 5), potentially orchestrating the response against influenza. *TDRD7* functions in a protein complex with TACC1, chTOG, Aurora A, and LSM7. Expressed RNAs of these proteins are colocalized in coexpression modules of all three species studied. The *TDRD7*-TACC1-chTOG-Aurora A complex orchestrates the regulation of microtubule dynamics, e.g., mitotic spindle organization and cell division (19). *TDRD7* has been identified to inhibit AMPK, which is essential for herpes simplex virus replication (15), and, successively, autophagy, a process that is required for paramyxovirus replication (16). However, IAV subverts autophagy to maintain virion stability for its life cycle (43). Thus, during IAV infections, the antiviral function of *TDRD7* may originate through the mediation of IFN replication and signaling. We have analyzed the consensus network neighborhood of *TDRD7* and have identified key targets that are affected by *TDRD7* KD (TDRD7<sup>KD</sup>). Among the *TDRD7*-enhanced ( $T^+$ ) targets are IFN-inducible GTPases *GBP1* and *GBP6*. The expression of *GBP6* in TDRD7<sup>KD</sup> cells at 24 hpi is at preinfection level, revoking the antiviral effect of this particular gene. Other IFN-inducible GTPases, such as *MX1* or *GBP1*, are similarly but less affected by TDRD7<sup>KD</sup>. Another ( $T^+$ ) target is *DPC2*. *DPC2* is known to modulate *IRF7* mRNA stability. However, we have not noticed a difference in *IRF7* expression between WT and TDRD7<sup>KD</sup> conditions. However, *IRF9* is affected, as well as *STAT1*. Thus, we presume that

*TDRD7* plays a role in the activation of ISG via the JAK/STAT/IRF9 pathway but does not affect IFN expression per se. Neither *IRF7* nor *IFNB1* is impaired by *TDRD7*<sup>KD</sup>. *TDRD7* may further modulate cell survival factors, such as *PIM1* and *BCL2A1*. *PIM1* then inhibits *AMPK*, affecting the viral life cycle.

The cross-species analysis further confirms the expected processes triggered during influenza infection. Early host defenses, particularly the innate immune response (TLR and IFN signaling and NK cell activation), are dominant and up-regulated in lung tissue. Down-regulated processes in the lung involve apoptotic signaling pathways, protein phosphorylation, or microtubule-based movement (see table S21 for a complete list of enriched GO terms). Blood-based neutrophil activation and vesicle transport were predominantly found up-regulated in blood. Nucleoplasmic genes and T cell activation processes were down-regulated in blood. Thus, the early host-defense mechanisms, such as apoptosis, and their inhibition by the virus take place at the location of the infection, the lungs. Conversely, the late state processes, such as the adaptive immune response, affect secondary “tissues,” such as blood. The comparative analysis between transcriptional response after IAV infection in lung and blood further shows that the early innate immune response is reacting and IFN response is up-regulated, while the host defense is quenched by the virus early in lung and late, as a secondary/systemic effect, in blood.

To identify species-specific molecular responses, we distinguish between sequence-based unique SRGs, i.e., SRGs with no homolog in other species, and function-based unique SRGs, i.e., genes that are present in more than one species but significantly expressed only in one species. Sequence-based unique SRGs constitute only 5 to 10% of all unique SRGs. Sequence-based human-specific SRGs include MHC class II DR genes, long intergenic and small nucleolar RNA, and other pseudogenes. Overall, sequence-based unique human DEGs contribute to the regulation of apoptosis and leukocyte activation. Determining what the sequence-based ferret-specific SRGs are is difficult because they are exclusive without annotations, while sequence-based mouse-specific SRGs are well-known ISGs and TLRs that are expressed in response to influenza infections, as in the case of *Tlr11* and *Tlr13*. *Tlr11* was shown to interact with flagellin (44) and respond against *Toxoplasma* infections (45). *Tlr13*, a receptor for bacterial RNA (46), was shown to recognize vesicular stomatitis virus (47) with further indications that it could identify influenza HA (48).

Network analysis provides further insights, particularly concerning unique processes across different systems. Unique human processes and corresponding network modules are predominantly involved in the regulation of the adaptive immune response, as indicated in the expression of truly unique MHC class II molecules such as *HLA-DRB*. For example, one unique human network is associated with negative regulation of leukocyte activation with immune response-suppressing MHC class I *HLA-G*, and another unique human network is involved in 5'-nucleotidase functionality and viral infectivity that promote NEXT-Exosome and endocannabinoid signaling function. The modulation of the airway response, increase of viral load, and attenuation of macrophages and CD4/CD8 T cells by  $\Delta^9$ -tetrahydrocannabinol have been well studied (49, 50). It seems that influenza may also attenuate the host immune response via this particular signaling pathway. This particular module is uniquely enriched for down-regulated genes during IAV infection. One particular target is up-regulated *NT5C2* with a network neighborhood significantly enriched for down-regulated genes in HTBE (FET  $P = 1.6 \times$

$10^{-31}$ , 13.9-fold). Another example of a human unique NWE regulator is the potential host defense gene *SPOCK2*, which is down-regulated with the significant down-regulated network neighborhood. Overall, these human unique processes tend to attenuate host defense and facilitate viral replication. Unique ferret processes assume a proviral role similar to the unique human processes. For example, one ferret's unique cell cycle network module includes mitochondrial maintenance complex genes with known proviral functions. Furthermore, unique ferret NWE regulators have been identified that are responsible for virus trafficking (*CLIP1*) and cytokine receptor and viral host factor *OSMR*. The mouse's unique processes potentially facilitate host defense. Mouse-specific modules are associated with down-regulated sphingolipid signaling pathway (including genes such as *Anxa11*, which is essential to viral processes), up-regulated positive regulation of T cell cytokine production, and up-regulated immune response network-enriched targets (e.g., *Slamf9* and *Pla2g7*), and they play an antiviral role during virus infection. *Anxa11* is essential to the cell cycle, apoptosis, vesicle trafficking, and signal transduction (27). Another mouse-specific module is associated with a down-regulated cyanate metabolic process composed of key genes such as *Dcxr*, *Mpst*, and *Tmem106c*. *Dcxr* plays an important role in sugar metabolism and detoxification and cell adhesion (51).

Our comprehensive cross-species comparative study provides novel insights into common and species-specific processes underlying influenza infection in three different mammalian species. We identified *TDRD7* as a prominent key regulator shared by the three species and experimentally validated it as an IFN-inducible host defense factor, whose depletion resulted in increased influenza virus growth in vitro and in vivo. We have presented evidence that *TDRD7* is required for IFN signaling and that *TDRD7* potentially modulates IFN response via the JAK/STAT/IRF9 pathway. The identification of key defense processes in mice, the revelation of human defense mechanisms, and the discovery of unique proviral host factors will facilitate the development of novel therapeutic interventions against influenza virus infection.

## MATERIALS AND METHODS

### Datasets

In this study, human whole blood, primary HTBE cells [NCBI Gene Expression Omnibus (GEO), accession number GSE89008], primary human MDM (NCBI GEO, accession number GSE97672), ferret blood, ferret upper and lower lung, and mouse lung (NCBI GEO, accession number GSE98527) were used.

### Human whole blood

Transcriptomic data were obtained from the NCBI GEO database using the influenza A-only subset of GSE40012. Whole blood samples were collected from critically ill individuals, suffering from H1N1 influenza A pneumonia, and assayed on Illumina HT-12 gene expression bead arrays.

### Ferrets

Tissues from two different lung quadrants (including one upper and one lower lung lobe) as well as blood were sampled from a total of 48 adult female ferrets, as part of the FluDyNeMo project ([www.synapse.org/fludynemo](http://www.synapse.org/fludynemo)).

### Viral plaque assay

Plaque assays were performed to determine the viral burden in lung tissue (52). Lung tissue supernatants were obtained from frozen

lung pieces that were gently thawed on ice, forced through a cell strainer (70  $\mu\text{m}$ ) and syringe plunger in PBS, and then spun down (2500 rpm, 5 min, 4°C) to collect the supernatant. Lung supernatants were diluted in Iscove's modified Dulbecco's minimum essential medium.

Madin-Darby canine kidney cells were plated ( $5 \times 10^5$ ) in each well of a six-well plate. Samples were diluted (final dilution factors of  $10^0$  to  $10^{-6}$ ) and overlaid onto the cells in 100  $\mu\text{l}$  of Dulbecco's modified Eagle's medium (DMEM) supplemented with penicillin-streptomycin and incubated for 1 hour. Samples were removed, cells were washed twice, and the medium was replaced with 2 ml of L15 medium plus 0.8% agarose (Cambrex, East Rutherford, NJ, USA) and incubated for 72 hours at 37°C with 5% carbon dioxide. Agarose was removed and discarded. The cells were fixed with 10% buffered formalin and then stained with 1% crystal violet for 15 min. After thorough washing in distilled water to remove excess crystal violet, the plates were dried, the number of plaques was counted, and the number of plaque-forming units (PFU) per milliliter was calculated.

### RNA-seq experiments

#### HTBE, MDM, and mouse lung

Cells were lysed in TRIzol (Thermo Fisher Scientific), and RNA was extracted either by adding chloroform, phase separation, and isolating RNA from the upper phase using RNeasy columns with on-column deoxyribonuclease (DNase) treatment (QIAGEN) or by using Direct-zol kits (Zymo Research) with on-column DNase treatment, following the manufacturer's instructions.

#### Ferret samples

RNA was extracted from ferret blood using the Mouse RiboPure-Blood RNA Isolation Kit (Ambion) and from ferret lungs using the RNeasy Mini Kit (QIAGEN). Both extraction methods followed the manufacturer's protocols and incorporated a DNase treatment (QIAGEN) after passing the sample through the filter cartridge. Strand-specific total RNA-seq libraries from ribosomal RNA-depleted RNA were prepared using the TruSeq Stranded Total RNA Library Prep Kit (Illumina) according to the manufacturer-supplied protocol. Libraries were sequenced 100 base pairs paired-end to a depth of approximately 40 million host genome reads on Illumina HiSeq 2500 instruments.

### Cells and viruses

HTBE cells were purchased from Lonza and passaged twice to generate a stock of cells stored in liquid nitrogen. Fully differentiated HTBE cells were used for viral infections. For differentiation, cells were amplified once in standard cell culture flasks and then seeded onto 12-mm-diameter Transwell filters (Corning) coated with collagen from human placenta (Sigma-Aldrich). Once confluent monolayers were formed on the filters, the medium was removed from the apical chamber, and cells were fed fresh medium only through the basolateral surface. At this time, retinoic acid (Sigma-Aldrich) at a final concentration of 50 nM was added to the medium. Cells were maintained in this way, with medium changed on Monday, Wednesday, and Friday for at least 4 weeks to allow differentiation. For the initial amplification of HTBE cells, bronchial epithelial growth medium, trypsin-EDTA, and Hepes-buffered saline solution from Lonza were used, according to the manufacturer's instructions. Upon seeding onto Transwell filters, cells were maintained in Gray's medium, a 1:1 mixture of bronchial epithelial basal medium and DMEM (Gibco), supplemented with growth factors and antimicrobials

included in a SingleQuots kit (Lonza). MDMs were prepared from buffy coats from anonymous healthy donor blood obtained from the New York Blood Center. Peripheral blood mononuclear cells were isolated by centrifugation on a Ficoll density gradient (Histopaque; Sigma-Aldrich), and CD14<sup>+</sup> cells were isolated using Miltenyi liquid separation mini columns and magnetic beads labeled with anti-human CD14 antibody (Miltenyi Biotec). For differentiation into macrophages, approximately 3 million CD14<sup>+</sup> monocytes were cultured for 10 days in RPMI 1640 (CellGro, Corning) containing 10% fetal bovine serum (HyClone; Thermo Fisher Scientific), 2 mM L-glutamine, 1 mM sodium pyruvate, and penicillin (100 U/ml)-streptomycin (100  $\mu\text{g}/\text{ml}$ ) (Gibco, Invitrogen) and supplemented with human granulocyte-macrophage colony-stimulating factor (1000 U/ml) (PeproTech).

A549 [American Type Culture Collection (ATCC), CCL-185], Madin-Darby canine kidney (MDCK) (ATCC CCL-34), HEK293T (ATCC, CRL-3216), and HTBE cells were cultured in DMEM supplemented with 10% FBS and penicillin-streptomycin (100 U/ml) at 37°C in 5% CO<sub>2</sub>. A/WSN/33 H1N1 virus was generated by reverse genetics and propagated in the allantoic cavity of embryonated chicken eggs. Titer was determined by plaque assay on MDCK cells using agar overlay medium.

### siRNA transfection

A549 or HTBE cells were transfected in suspension with siRNAs at 20 nM (Dharmacon) using the RNAiMAX reagent according to the manufacturer's protocol (Invitrogen). At 48 hours after transfection, cells were either infected, RNA was isolated and subjected to quantitative reverse transcription polymerase chain reaction, or cell viability was determined using the CellTiter-Glo assay (Promega).

### Virus infection

A549 cells were infected with the virus at the indicated multiplicity of infection in PBS supplemented with bovine serum albumin (BSA) and Ca<sup>2+</sup>/Mg<sub>2</sub>. After 1 hour, viral inoculum was removed and cells were washed. For A549 culture, medium containing TPCK-treated trypsin (1  $\mu\text{g}/\text{ml}$ ) was added. Cells were then incubated at 37°C, and supernatant samples were collected at indicated times. Viral titer in supernatants was determined by plaque assay using MDCK cells. For HTBE cells, culture medium was added, and cell lysates were collected at indicated times after infection and subjected to RNA-seq.

### PPMO design for TDRD7 KD

PPMOs were produced as described before (53). Two PPMOs were designed against the TDRD7 gene; PPMO1: TDRD7-AUG (GATCTGCCTCCAGCATCTTTGCC) targets the start codon region of the mRNA and PPMO2: TDRD7-793 e5i5 (CATGCACATCTGGAGAACATACCAT) targets an intron-exon junction of the pre-mRNA. A nontargeting PPMO control sequence (Scr PPMO) (CCTCTTACCTCAGTTACAATTTATA), having little homology to mouse transcripts or influenza viral sequences, was used as control. PPMO1 and PPMO2 were tested in mouse embryonic fibroblast for their efficacy in knocking down TDRD7 protein expression. Eventually, for in vivo experiments, an equimolar mix of PPMO1 and PPMO2 was used.

### Animal experiments

Five-week-old female BALB/c mice were purchased from the Jackson Laboratory. Mice were anesthetized by intraperitoneal injection of a

mixture of ketamine and xylazine (100 and 5  $\mu\text{g}$  per gram of body weight), before intranasal administration of either PBS or 100  $\mu\text{mol}$  of PPMO mix (50  $\mu\text{mol}$  of PPMO1 and PPMO2 each) in 40  $\mu\text{l}$  of PBS, on day  $-2$  and day  $-1$ . On day 0, mice were challenged intranasally with 40 PFU of PR8 IAV [ $\text{LD}_{50}$  (median lethal dose) = 50 PFU] in 40  $\mu\text{l}$  of PBS. Mice were monitored daily for weight loss and clinical signs. Mouse lungs were harvested on day 3 and day 6 after infection for measuring viral titers (five mice per condition). Lung homogenates were prepared using a FastPrep24 system (MP Bio-medicals). After the addition of 800  $\mu\text{l}$  of PBS containing 0.3% BSA, the lungs were subjected to two rounds of mechanical treatment for 10 s each at 6.5 m/s. Tissue debris was removed by low-speed centrifugation, and virus titers in supernatants were determined by plaque assay.

Female Fitch ferrets (*Mustela putorius furo*) were obtained from Triple F Farms (Sayre, PA) and were seronegative to circulating influenza A (H1N1 and H3N2) and influenza B viruses. Adult ferrets ( $n = 48$ ), 6 to 12 months of age, were pair-housed in stainless steel cages (Shor-Line, Kansas City, KS) that contained Sani-Chips laboratory animal bedding (P.J. Murphy Forest Products, Montville, NJ) and provided with food and fresh water ad libitum. To achieve a mean of 20% weight loss no earlier than 8 dpi, adult ferrets were infected intranasally with H1N1pdm09 virus A/California/07/2009 at a dose of  $10^6$  PFU. The animals were monitored daily for the severity of clinical disease using weight loss. Disease symptoms, including elevated temperature, low activity level, sneezing, and nasal discharge, were noted if present. Any animal reaching  $>20\%$  weight loss was humanely euthanized. Ferrets were randomly assigned to be removed from the study at 1, 3, 5, and 8, dpi, and lung tissues were collected unless their clinical conditions (e.g., loss of  $>20\%$  body weight) required a humane end point. Blood was collected from anesthetized ferrets via the anterior vena cava after infection. Serum was harvested and frozen at a mean  $\pm$  SD of  $-20^\circ \pm 5^\circ\text{C}$ . The University of Georgia Institutional Animal Care and Use Committee approved all experiments, which were conducted in accordance with the National Institutes of Health's (NIH's) *Guide for the Care and Use of Laboratory Animals* (52), the Animal Welfare Act, and the Biosafety in Microbiological and Biomedical Laboratories guide of the Centers for Disease Control and Prevention and the NIH.

### Ethics statement

All research studies involving the use of animals were reviewed and approved by the Institutional Animal Care and Use Committees of the Icahn School of Medicine at Mount Sinai and the University of Georgia. Studies were carried out in strict accordance with the recommendations in the *Guide for the Care and Use of Laboratory Animals*.

### RNA-seq analysis

Paired reads of the ferret RNA-seq data were aligned to the ferret genome Ensembl version 1.0.80 using tophat (v2.0.13). Reads were summarized and assigned to genomic features by featureCounts v2.0.1. Raw counts after featureCount as well as from the raw RNA-seq datasets obtained from GEO were further processed using the edgeR v3.30.0/limma v3.4.4.1 pipeline with R v4.0.0. Counts were further normalized, batch-corrected using a robust linear model with the confounding factors, and quality-controlled. The edgeR/limma pipeline was further used to identify DEGs. Genes were considered significantly differentially expressed with  $\text{FC} \geq 1.5$  or  $\text{FC} \leq 1/1.5$

and adjusted  $P$  value  $\leq 0.05$  (adjusted for multiple testing by Benjamini and Hochberg).

### Comparative analysis and set algebra

We performed comparative analyses on eight different groups of interest, involving two tissues (blood and lung tissue), three species (humans, ferrets, and mice), and different model systems (a model system refers to the specific compartment of a tissue of a specific species, e.g., ferret upper lung, lower lung, MDMs, or human HTBE cells) (fig. S1). The set union has been used when referring to overall responses, e.g., from lungs, of different organisms, whereas the set intersection was used when referring to conserved responses.

### Identification of DEGs

Given the time series information for each different dataset, we used two distinct methods to identify DEGs. We used a generalized linear model together with an analysis of variance (ANOVA)-like quasi-likelihood  $F$  test as implemented in the edgeR package (54) to identify DEGs across the time series, termed SRGs. Significance is defined based on an FDR of 5% or less and using an effect size calculated after variance explained and an  $\eta^2 \geq 0.06$ . In addition, we used a complementary nonparametric JTA (55) to identify significantly up- or down-regulated genes (JTGs) across early measured time points at an FDR of 10% or less, which was chosen to yield a significant number of JTGs in each dataset analyzed. DEGs are used as a generic term for differentially expressed genes, including SRGs and JTGs. Early in vivo response was determined in the first 2 days. Such a clear definition was needed to prevent a biased interpretation of directional up- or down-regulation due to the return to baseline of expression responses after viral clearance at later time points. Time series data of signature genes are provided as reference in the Supplementary Materials.

### Gene coexpression network analysis

MEGENA (14) was performed to identify host modules of highly coexpressed genes in influenza infection. The MEGENA workflow comprises four major steps: (i) fast planar filtered network construction, (ii) multiscale clustering analysis, (iii) multiscale hub analysis, and (iv) cluster-trait association analysis. The total relevance of each consensus module to influenza infection was calculated by summarizing the combined enrichment of the DEG signatures and trait correlations:  $G_j = \prod_i g_{ji}$ , where  $g_{ji}$  is the relevance of a consensus  $j$  to a signature  $i$ , and  $g_{ji}$  is defined as  $(\max_j(r_{ji}) + 1 - r_{ji}) / \sum_j r_{ji}$ , where  $r_{ji}$  is the ranking order of the significance level of the overlap between the consensus module  $j$  and the signature  $i$ . MEGENA was applied to each dataset in each system independently, and all the genes profiled in each dataset were used for network construction.

### Identification of enriched pathways and hub genes in the host modules

To functionally annotate gene signatures and gene modules identified in this study, we performed an enrichment analysis of the established pathways and signatures—including the GO (56) biological processes category and MSigDB (57) canonical pathways (C2.CP)—and the subject area-specific gene sets—including influenza host factors (58, 59), inflammasome, interferome, and InnateDB. Enrichment analysis was performed using FET (in-house and the hypergeometric test from the Category R package). The hub genes in each

subnetwork were identified using the adopted Fisher's inverse chi-square approach in MEGENA; Bonferroni-corrected  $P$  values smaller than 0.05 were set as the threshold to identify significant hubs.

### Key regulator identification (60, 61)

The analysis to identify key regulators takes as input a set of genes ( $G$ ) and a coexpression network. The objective is to identify the key regulators for the gene sets with respect to the given network. This approach first generates a subnetwork  $NG$ , defined as the set of nodes in  $N$  that are no more than  $h$  layers away from the nodes in  $G$ , and then searches the  $h$  layer neighborhood (HLN) ( $h = 1, \dots, H$ ) for each gene in  $NG$  ( $HLN_{g,h}$ ) for the optimal  $h^*$ , such that

$$ES_h^* = \max(ES_{h,g}) \forall g \in N_g, h \in \{1, \dots, H\}$$

where  $ES_{h,g}$  is the computed enrichment statistic for  $HLN_{g,h}$ . A node becomes a candidate driver if its HLN is significantly enriched for the nodes in  $G$ . Candidate drivers without any parent node (i.e., root nodes in directed networks) are designated as global drivers and the rest are local drivers. To identify the system-specific key regulators in their coexpression networks, the corresponding SRGs have been used as gene set  $G$ .

### Network enrichment

FET was performed to determine the overlap between network neighborhoods of potential key regulators (target) and an input DEG signature. For each target in the network in the 95th percentile of node strength after MEGENA, the genes in the network neighborhoods between one and four steps away from the target were intersected with the DEG signature (e.g., SRG signatures as well as up- and down-regulated JTG signatures). MEGENA networks of all systems were tested with DEGs of all systems for further analysis (see the section "TDRD7 is an IFN Induced Common Defense Factor and Key Regulator against Influenza Infection"). Cumulative network enrichment scores  $s = 1/n \cdot \sum_i -\log_{10} P_i$  based on individual FET  $P$  values for each target and specific scenarios [shown in figs. S2 (E and F) to S6 (E and F) and S20] were calculated.  $n$  is the number of realizations (i.e., the number of different neighborhoods and systems used to calculate the particular score). Significantly different network scores  $\sigma_i = -\log_{10} P_i$  between scenarios for individual targets were identified after  $t$  test, using an FDR of 5% or less and a "fold (score) change" between scores of 2 or more.

### Unique genes SUGs and FUGs

To define unique genes between species, we considered two different scenarios: SUGs and FUGs. For a given species  $x$ , SUGs are the genes in  $x$  that have no ortholog in any other species investigated in this study, while FUGs are those that have orthologs in other species but are functionally specific to  $x$  regarding responses to IAV infections. Function refers to differential expression and a prominent role in gene subnetworks associated with physiology and phenotypes induced by IAV infections. We used one-on-one orthologs available from the NCBI ortholog information. Within NCBI, ortholog gene groups are calculated by NCBI's Eukaryotic Genome Annotation pipeline for the NCBI gene dataset using a combination of protein sequence similarity (including percent coverage) and local synteny information.

### Graphic data presentation

Heatmaps showing gene set enrichments were produced using the moduleGO functions from the R package DGCA (differential gene correlation analysis) (62). The circos plot was constructed using the NetWeaver R package. Gene coexpression networks were visualized with CytoScape (63).

### SUPPLEMENTARY MATERIALS

Supplementary material for this article is available at <https://science.org/doi/10.1126/sciadv.abm5859>

[View/request a protocol for this paper from Bio-protocol.](#)

### REFERENCES AND NOTES

- World Health Organization, Influenza (Seasonal) Fact Sheet: World Health Organization (2018); [www.who.int/news-room/fact-sheets/detail/influenza-\(seasonal\)](http://www.who.int/news-room/fact-sheets/detail/influenza-(seasonal)).
- B. N. Fields, D. M. Knipe, P. M. Howley, D. E. Griffin, *Fields Virology* (Lippincott Williams & Wilkins, ed. 4, 2001).
- T. P. Monie, *The Innate Immune System* (Elsevier, 2017).
- A. Pichlmair, M. Habjan, H. Unger, F. Weber, Virus-like particles expressing the nucleocapsid gene as an efficient vaccine against Rift Valley fever virus. *Vector Borne Zoonotic Dis.* **10**, 701–703 (2010).
- M. Schlee, A. Roth, V. Hornung, C. A. Hagmann, V. Wimmenauer, W. Barchet, C. Coch, M. Janke, A. Mihailovic, G. Wardle, S. Juraneck, H. Kato, T. Kawai, H. Poeck, K. A. Fitzgerald, O. Takeuchi, S. Akira, T. Tuschl, E. Latz, J. Ludwig, G. Hartmann, Recognition of 5' triphosphate by RIG-I helicase requires short blunt double-stranded RNA as contained in panhandle of negative-strand virus. *Immunity* **31**, 25–34 (2009).
- H. Poeck, M. Bscheider, O. Gross, K. Finger, S. Roth, M. Rebsamen, N. Hahnenschläger, M. Schlee, S. Rothenfusser, W. Barchet, H. Kato, S. Akira, S. Inoue, S. Endres, C. Peschel, G. Hartmann, V. Hornung, J. Ruland, Recognition of RNA virus by RIG-I results in activation of CARD9 and inflammasome signaling for interleukin 1 beta production. *Nat. Immunol.* **11**, 63–69 (2010).
- Y. M. Loo, J. Fornek, N. Crochet, G. Bajwa, O. Perwitasari, L. Martinez-Sobrido, S. Akira, M. A. Gill, A. Garcia-Sastre, M. G. Katze, M. Gale Jr., Distinct RIG-I and MDA5 signaling by RNA viruses in innate immunity. *J. Virol.* **82**, 335–345 (2008).
- N. M. Bouvier, A. C. Lowen, Animal models for influenza virus pathogenesis and transmission. *Viruses* **2**, 1530–1563 (2010).
- I. Margine, F. Krammer, Animal models for influenza viruses: Implications for universal vaccine development. *Pathogens* **3**, 845–874 (2014).
- C. E. Bryant, T. P. Monie, Mice, men and the relatives: Cross-species studies underpin innate immunity. *Open Biol.* **2**, 120015 (2012).
- J. Seok, H. S. Warren, A. G. Cuenca, M. N. Mindrinos, H. V. Baker, W. Xu, D. R. Richards, G. McDonald-Smith, H. Gao, L. Hennessy, C. C. Finnerty, C. M. López, S. Honari, E. E. Moore, J. P. Minei, J. Cuschieri, P. E. Bankay, J. L. Johnson, J. Sperry, A. B. Nathens, T. R. Billiar, M. A. West, M. G. Jeschke, M. B. Klein, R. L. Gamelli, N. S. Gibran, B. H. Brownstein, C. Miller-Graziano, S. E. Calvano, P. H. Mason, J. P. Cobb, L. G. Rahme, S. F. Lowry, R. V. Maier, L. L. Moldawer, D. N. Herndon, R. W. Davis, W. Xiao, R. G. Tompkins; Inflammation and Host Response to Injury, Large Scale Collaborative Research Program, Genomic responses in mouse models poorly mimic human inflammatory diseases. *Proc. Natl. Acad. Sci. U.S.A.* **110**, 3507–3512 (2013).
- R. Rajsbaum, R. A. Albrecht, M. K. Wang, N. P. Maharaj, G. A. Versteeg, E. Nistal-Villán, A. Garcia-Sastre, M. U. Gack, Species-specific inhibition of RIG-I ubiquitination and IFN induction by the influenza A virus NS1 protein. *PLoS Pathog.* **8**, e1003059 (2012).
- M. Wang, Y. Zhao, B. Zhang, Efficient test and visualization of multi-set intersections. *Sci. Rep.* **5**, 16923 (2015).
- W. M. Song, B. Zhang, Multiscale embedded gene co-expression network analysis. *PLoS Comput. Biol.* **11**, e1004574 (2015).
- G. Subramanian, S. Popli, S. Chakravarty, R. T. Taylor, R. Chakravarti, S. Chattopadhyay, The interferon-inducible protein TDRD7 inhibits AMP-activated protein kinase and thereby restricts autophagy-independent virus replication. *J. Biol. Chem.* **295**, 6811–6822 (2020).
- G. Subramanian, T. Kuzmanovic, Y. Zhang, C. B. Peter, M. Veleeparambil, R. Chakravarti, G. C. Sen, S. Chattopadhyay, A new mechanism of interferon's antiviral action: Induction of autophagy, essential for paramyxovirus replication, is inhibited by the interferon stimulated gene, TDRD7. *PLoS Pathog.* **14**, e1006877 (2018).
- N. M. Held, R. H. Houtkooper, Mitochondrial quality control pathways as determinants of metabolic health. *Bioessays* **37**, 867–876 (2015).
- D. Szklarczyk, J. H. Morris, H. Cook, M. Kuhn, S. Wyder, M. Simonovic, A. Santos, N. T. Doncheva, A. Roth, P. Bork, L. J. Jensen, C. von Mering, The STRING database in 2017:

- Quality-controlled protein-protein association networks, made broadly accessible. *Nucleic Acids Res.* **45**, D362–D368 (2017).
19. N. Conte, B. Delaval, C. Ginestier, A. Ferrand, D. Isnardon, C. Larroque, C. Prigent, B. Séraphin, J. Jacquemier, D. Birnbaum, TACC1–chTOG–Aurora A protein complex in breast cancer. *Oncogene* **22**, 8102–8116 (2003).
  20. P. Anderson, N. Kedersha, RNA granules: Post-transcriptional and epigenetic modulators of gene expression. *Nat. Rev. Mol. Cell Biol.* **10**, 430–436 (2009).
  21. M. K. Duncan, Development. A new focus on RNA in the lens. *Science* **331**, 1523–1524 (2011).
  22. N. Pobleto-Duran, Y. Prades-Pérez, J. Vera-Otarola, R. Soto-Rifo, F. Valiente-Echeverría, Who regulates whom? An overview of rna granules and viral infections. *Viruses* **8**, 180 (2016).
  23. M. Lubas, M. S. Christensen, M. S. Kristiansen, M. Domanski, L. G. Falkenby, S. Lykke-Andersen, J. S. Andersen, A. Dziembowski, T. H. Jensen, Interaction profiling identifies the human nuclear exosome targeting complex. *Mol. Cell* **43**, 624–637 (2011).
  24. A. Rialdi, J. Hultquist, D. Jimenez-Morales, Z. Peralta, L. Campisi, R. Fenouil, N. Moshkina, Z. Z. Wang, B. Laffleur, R. M. Kaake, M. J. McGregor, K. Haas, E. Pefanis, R. A. Albrecht, L. Pache, S. Chanda, J. Jen, J. Ochando, M. Byun, U. Basu, A. García-Sastre, N. Krogan, H. van Bakel, I. Marazzi, The RNA exosome syncs IAV-RNAPII transcription to promote viral ribogenesis and infectivity. *Cell* **169**, 679–692.e14 (2017).
  25. C. V. Forst, B. Zhou, M. Wang, T. W. Chou, G. Mason, W. M. Song, E. Schadt, E. Ghedin, B. Zhang, Integrative gene network analysis identifies key signatures, intrinsic networks and host factors for influenza virus A infections. *NPJ Syst. Biol. Appl.* **3**, 35 (2017).
  26. Z. W. Lee, L. W. Deng, Role of H2S donors in cancer biology. *Handb. Exp. Pharmacol.* **230**, 243–265 (2015).
  27. S. Liu, C. Guo, J. Wang, B. Wang, H. Qi, M. Z. Sun, ANXA11 regulates the tumorigenesis, lymph node metastasis and 5-fluorouracil sensitivity of murine hepatocarcinoma Hca-P cells by targeting c-Jun. *Oncotarget* **7**, 16297–16310 (2016).
  28. Q. Wang, Q. Li, R. Liu, M. Zheng, J. Wen, G. Zhao, Host cell interactome of PA protein of H5N1 influenza A virus in chicken cells. *J. Proteomics* **136**, 48–54 (2016).
  29. N. Ahn, J.-Y. Yoo, ID: 125: Identification of novel proteoglycan that inhibits influenza virus replication. *Cytokine* **76**, 89 (2015).
  30. N. Ahn, W. J. Kim, N. Kim, H. W. Park, S. W. Lee, J. Y. Yoo, The interferon-inducible proteoglycan Testican-2/SPOCK2 functions as a protective barrier against virus infection of lung epithelial cells. *J. Virol.* **93**, e00662-19 (2019).
  31. W. Emanuel, M. Kirstin, F. Vedran, D. Asija, G. L. Theresa, A. Roberto, K. Filippou, K. David, A. Salah, B. Christopher, R. Anja, L. Ivano, I. Andranik, M. Tommaso, D. G. Simone, P. J. Patrick, M. M. Alexander, N. Daniela, S. Matthias, A. Altuna, R. Nikolaus, D. Christian, L. Markus, Bulk and single-cell gene expression profiling of SARS-CoV-2 infected human cell lines identifies molecular targets for therapeutic intervention. bioRxiv 2020.05.05.079194 [Preprint]. 5 May 2020. <https://doi.org/10.1101/2020.05.05.079194>.
  32. Y. Zheng, Z. Y. Lin, J. J. Xie, F. N. Jiang, C. J. Chen, J. X. Li, X. Zhou, W. D. Zhong, ARRD3C inhibits the progression of human prostate cancer through ARRD3C-ITGB4 pathway. *Curr. Mol. Med.* **17**, 221–229 (2017).
  33. K. M. Draheim, H. B. Chen, Q. Tao, N. Moore, M. Roche, S. Lyle, ARRD3C suppresses breast cancer progression by negatively regulating integrin beta4. *Oncogene* **29**, 5032–5047 (2010).
  34. D. P. Dowlatshahi, V. Sandrin, S. Vivona, T. A. Shaler, S. E. Kaiser, F. Melandri, W. I. Sundquist, R. R. Kopito, ALIX is a Lys63-specific polyubiquitin binding protein that functions in retrovirus budding. *Dev. Cell.* **23**, 1247–1254 (2012).
  35. M. R. Dores, H. Lin, N. J. Grimsey, F. Mendez, J. A. Trejo, The  $\alpha$ -arrestin ARRD3C mediates ALIX ubiquitination and G protein-coupled receptor lysosomal sorting. *Mol. Biol. Cell* **26**, 4660–4673 (2015).
  36. A. J. Sadler, B. R. Williams, Interferon-inducible antiviral effectors. *Nat. Rev. Immunol.* **8**, 559–568 (2008).
  37. Y.-C. Liu, B. W.-Y. Mok, P. Wang, R.-L. Kuo, H. Chen, S.-R. Shih, Cellular 5'-3' mRNA exoribonuclease XRN1 inhibits interferon beta activation and facilitates influenza A virus replication. *mBio* **12**, e00945–21 (2021).
  38. Y. Li, J. Dai, M. Song, P. Fitzgerald-Bocarsly, M. Kiledjian, Dcp2 decapping protein modulates mRNA stability of the critical interferon regulatory factor (IRF) IRF-7. *Mol. Cell Biol.* **32**, 1164–1172 (2012).
  39. E. C. Tom, I. Mushtaq, B. C. Mohapatra, H. Luan, A. M. Bhat, N. Zutshi, S. Chakraborty, N. Islam, P. Arya, T. A. Bielecki, F. M. Iseka, S. Bhattacharyya, L. R. Cypher, B. T. Goetz, S. K. Negi, M. D. Storck, S. Rana, A. Barnekow, P. K. Singh, G. Ying, C. Guda, A. Natarajan, V. Band, H. Band, EHD1 and RUSC2 control basal epidermal growth factor receptor cell surface expression and recycling. *Mol. Cell Biol.* **40**, e00434-19 (2020).
  40. M. Szydłowski, S. Dębek, M. Prochorec-Sobieszek, M. Szołkowska, A. M. Tomirotti, P. Juszczyński, A. Szumera-Ciećkiewicz, PIM kinases promote survival and immune escape in primary mediastinal large B-cell lymphoma through modulation of JAK-STAT and NF- $\kappa$ B activity. *Am. J. Pathol.* **191**, 567–574 (2021).
  41. M. de Vries, N. P. Smithers, P. H. Howarth, M. C. Nawijn, D. E. Davies, Inhibition of Pim1 kinase reduces viral replication in primary bronchial epithelial cells. *Eur. Respir. J.* **45**, 1745–1748 (2015).
  42. K. L. Mung, W. B. Eccleshall, N. M. Santio, A. Rivero-Müller, P. J. Koskinen, PIM kinases inhibit AMPK activation and promote tumorigenicity by phosphorylating LKB1. *Cell Commun. Sig.* **19**, 68 (2021).
  43. R. Beale, H. Wise, A. Stuart, B. J. Ravenhill, P. Digard, F. Randow, A LC3-interacting motif in the influenza A virus M2 protein is required to subvert autophagy and maintain virion stability. *Cell Host Microbe* **15**, 239–247 (2014).
  44. H. Hatai, A. Lepelley, W. Zeng, M. S. Hayden, S. Ghosh, Toll-like receptor 11 (TLR11) interacts with flagellin and profilin through disparate mechanisms. *PLOS ONE* **11**, e0148987 (2016).
  45. M. Pepper, F. Dzierszinski, E. Wilson, E. Tait, Q. Fang, F. Yarovsky, T. M. Laufer, D. Roos, C. A. Hunter, Plasmacytoid dendritic cells are activated by *Toxoplasma gondii* to present antigen and produce cytokines. *J. Immunol.* **180**, 6229–6236 (2008).
  46. A. Hidmark, A. von Saint Paul, A. H. Dalpke, Cutting edge: TLR13 is a receptor for bacterial RNA. *J. Immunol.* **189**, 2717–2721 (2012).
  47. Z. Shi, Z. Cai, A. Sanchez, T. Zhang, S. Wen, J. Wang, J. Yang, S. Fu, D. Zhang, A novel Toll-like receptor that recognizes vesicular stomatitis virus. *J. Biol. Chem.* **286**, 4517–4524 (2011).
  48. S. Marshall-Clarke, L. Tasker, O. Buchatska, J. Downes, J. Pennock, S. Wharton, P. Borrow, D. Z. Wiseman, Influenza H2 haemagglutinin activates B cells via a MyD88-dependent pathway. *Eur. J. Immunol.* **36**, 95–106 (2006).
  49. J. P. Buchweitz, P. W. Karmaus, J. R. Harkema, K. J. Williams, N. E. Kaminski, Modulation of airway responses to influenza A/PR/8/34 by Delta9-tetrahydrocannabinol in C57BL/6 mice. *J. Pharmacol. Exp. Ther.* **323**, 675–683 (2007).
  50. C. S. Reiss, Cannabinoids and viral infections. *Pharmaceuticals (Basel)* **3**, 1873–1886 (2010).
  51. B. Ebert, M. Kisiela, E. Maser, Human DCXR—Another 'moonlighting protein' involved in sugar metabolism, carbonyl detoxification, cell adhesion and male fertility? *Biol. Rev. Camb. Philos. Soc.* **90**, 254–278 (2015).
  52. S. J. Bissel, C. E. Carter, G. Wang, S. K. Johnson, L. P. Lashua, A. A. Kelvin, C. A. Wiley, E. Ghedin, T. M. Ross, Age-related pathology associated with H1N1 A/California/07/2009 influenza virus infection. *Am. J. Pathol.* **189**, 2389–2399 (2019).
  53. S. Abes, H. M. Moulton, P. Clair, P. Prevot, D. S. Youngblood, R. P. Wu, P. L. Iversen, B. Lebleu, Vectorization of morpholino oligomers by the (R-Ahx-R)4 peptide allows efficient splicing correction in the absence of endosomolytic agents. *J. Control. Release* **116**, 304–313 (2006).
  54. M. D. Robinson, D. J. McCarthy, G. K. Smyth, edgeR: A bioconductor package for differential expression analysis of digital gene expression data. *Bioinformatics* **26**, 139–140 (2010).
  55. A. R. Jonckheere, A distribution-free  $k$ -sample test against ordered alternatives. *Biometrika* **41**, 133–145 (1954).
  56. Gene Ontology Consortium, Gene Ontology Consortium: Going forward. *Nucleic Acids Res.* **43**, D1049–D1056 (2015).
  57. A. Subramanian, P. Tamayo, V. K. Mootha, S. Mukherjee, B. L. Ebert, M. A. Gillette, A. Paulovich, S. L. Pomeroy, T. R. Golub, E. S. Lander, J. P. Mesirov, Gene set enrichment analysis: A knowledge-based approach for interpreting genome-wide expression profiles. *Proc. Natl. Acad. Sci. U.S.A.* **102**, 15545–15550 (2005).
  58. T. Watanabe, S. Watanabe, Y. Kawaoka, Cellular networks involved in the influenza virus life cycle. *Cell Host Microbe* **7**, 427–439 (2010).
  59. S. Tripathi, M. O. Pohl, Y. Zhou, A. Rodriguez-Frandsen, G. Wang, D. A. Stein, H. M. Moulton, P. DeJesus, J. Che, L. C. F. Mulder, E. Yáñez, D. Andenmatten, L. Pache, B. Manicassamy, R. A. Albrecht, M. G. Gonzalez, Q. Nguyen, A. Brass, S. Elledge, M. White, S. Shapira, N. Hacoen, A. Karlas, T. F. Meyer, M. Shales, A. Gatorano, J. R. Johnson, G. Jiang, T. Johnson, E. Verschuere, D. Sanders, N. Krogan, M. Shaw, R. König, S. Stertz, A. García-Sastre, S. K. Chanda, Meta- and orthogonal integration of influenza "OMICs" data defines a role for UBR4 in virus budding. *Cell Host Microbe* **18**, 723–735 (2015).
  60. L. A. Peters, J. Perrigou, A. Mortha, A. Iuga, W. M. Song, E. M. Neiman, S. R. Llewellyn, A. di Narzo, B. A. Kidd, S. E. Telesco, Y. Zhao, A. Stojimirovic, J. Sendekci, K. Shameer, R. Miotto, B. Losic, H. Shah, E. Lee, M. Wang, J. J. Faith, A. Kasarskis, C. Brodmerkel, M. Curran, A. das, J. R. Friedman, Y. Fukui, M. B. Humphrey, B. M. Iritani, N. Sibinga, T. K. Tarrant, C. Argmann, K. Hao, P. Roussos, J. Zhu, B. Zhang, R. Dobrin, L. F. Mayer, E. E. Schadt, A functional genomics predictive network model identifies regulators of inflammatory bowel disease. *Nat. Genet.* **49**, 1437–1449 (2017).
  61. B. Zhang, J. Zhu, Identification of key causal regulators in gene networks, in *Proceedings of the World Congress on Engineering (IAENG)*, (2013), pp. 1309–1312.
  62. A. T. McKenzie, I. Katsy, W. M. Song, M. Wang, B. Zhang, DGCA: A comprehensive R package for differential gene correlation analysis. *BMC Syst. Biol.* **10**, 106 (2016).

63. P. Shannon, A. Markiel, O. Ozier, N. S. Baliga, J. T. Wang, D. Ramage, N. Amin, B. Schwikowski, T. Ideker, Cytoscape: A software environment for integrated models of biomolecular interaction networks. *Genome Res.* **13**, 2498–2504 (2003).
64. S. E. Ward, H. S. Kim, K. Komurov, S. Mendiratta, P. L. Tsai, M. Schmolke, N. Satterly, B. Manicassamy, C. V. Forst, M. G. Roth, A. García-Sastre, K. M. Blazewska, C. E. McKenna, B. M. Fontoura, M. A. White, Host modulators of H1N1 cytopathogenicity. *PLOS ONE* **7**, e39284 (2012).

#### Acknowledgments

**Funding:** This work was funded by National Institutes of Health grant R21 AI149013 (to C.V.F.), National Institutes of Health grant U01 AI111598 (to B.Z. and E.G.), National Institutes of Health grant U19 AI106754 (to A.G.-S., M.L.S., and S.K.C.), and National Institutes of Health grant U19 AI135972 (to A.G.-S., L.P., and S.K.C.). This work was also funded in part by the Division of Intramural Research (DIR) of NIAID/NIH (to E.G.) and by NIAID grants U19AI142733 and U19AI168631, CRIPT (Center for Research on Influenza Pathogenesis and Transmission), and NIAID-funded Center of Excellence for Influenza Research and Response (CEIRR; contract #75N93021C00014) to A.G.-S. S.T. is supported by the DBT-Wellcome Trust India Alliance Intermediate Fellowship (IA/I/18/1/503613). The A.G.-S. laboratory has received research support from Pfizer, Senhwa Biosciences, Kenall Manufacturing, Avimex, Johnson & Johnson, Dynavax, 7 Hills Pharma, Pharmamar, ImmunityBio, Accurius, Nanocompositix, Hexamer, N-fold LLC, Model Medicines, Atea Pharma, Applied Biological Laboratories, and Merck, outside of the

reported work. A.G.-S. has consulting agreements for the following companies involving cash and/or stock: Vivaldi Biosciences, Contrafect, 7 Hills Pharma, Avimex, Vaxalto, Pagoda, Accurius, Esperovax, Farmak, Applied Biological Laboratories, Pharmamar, Paratus, CureLab Oncology, CureLab Veterinary, Synairgen, and Pfizer, outside of the reported work. **Author contributions:** Conceptualization: C.V.F., E.G., and B.Z. Investigation: C.V.F., L.M.-S., and S.T. Data analysis: C.V.F., M.W., X.Z., and L.P. Experiment design: M.L.S., H.M., T.M.R., E.G., S.K.C., and A.G.-S. Experiments: L.M.-S., S.T., G.W., L.G.D.A.B., A.G., L.L., T.D., C.E.C., G.M., A.R.-F., M.D.U., K.M.W., and D.A.S. Writing—original draft and editing: C.V.F., A.G.-S., E.G., and B.Z. Writing—review: All authors. **Competing interests:** A.G.-S. is an inventor on patents and patent applications on the use of antivirals and vaccines for the treatment and prevention of virus infections and cancer, owned by the Icahn School of Medicine at Mount Sinai, New York, outside of the reported work. All other authors declare that they have no competing interests. **Data and materials availability:** All data needed to evaluate the conclusions in the paper are present in the paper, the Supplementary Materials, and/or online. RNA-seq data are available at GEO under accession numbers GSE89008, GSE97672, GSE98527, and GSE168512. Data and code can be accessed at Synapse.org (DOI: 10.7303/syn26251888).

Submitted 28 September 2021

Accepted 11 August 2022

Published 5 October 2022

10.1126/sciadv.abm5859